INTERNATIONAL ATOMIC ENERGY AGENCY
UNITED NATIONS EDUCATIONAL, SCIENTIFIC AND CULTURAL ORGANIZATION

INTERNATIONAL CENTRE FOR THEORETICAL PHYSICS
34100 TRIESTE (ITALY) - P.O.B. 586 - MIRAMARE - STRADA COSTIERA 11 - TELEPHONE: 2240-1
CABLE: CENTRATOM - TELEX 460392-1

H4.SMR.203 - 37

" SPRING COLLEGE ON GEOMAGNETISM AND AERONOMY "

(2 - 27 March 1987)

" Equatorial electrojet " I and II

presented by :

R.G. RASTOGI
Indian Institute of Geomagnetism
Dr. Nanabhoy Moos Road
Colaba
Bombay 400 005
India

Lecture Notes
by
R. G. Rastogi
on
Equatorial Electrojet I and II

Regular daily variations of the geomagnetic field components have been known from the very early data from geomagnetic observatories and these variations have been attributed to electric currents in the upper atmosphere. The establishment of geomagnetic observatory at Huancayo in 1922 showed an abnormally large solar daily variation at equatorial latitude and was attributed to very strong eastward currents during the daytime overhead the station. The establishment of few additional observatories at low latitudes led to the discovery of the enhancement of the daily variation over the dip equator within a very narrow belt of $\pm 5°$ (Egedal 1944). This enhanced eastward current was named by Prof Chapman as EQUATORIAL ELECTROJET.

In Fig 1(a) and 1(b) are shown the location of geomagnetic observatories in Indo-USSR longitudes and the solar quiet day variations of the Horizontal (H) and Vertical (Z) components of the geomagnetic field as well as of the Declination at these observatories

Fig 1(a) and 1(b)

The latitudinal variations of the amplitude and phase of the diurnal and semi diurnal components of the daily variations of these geomagnetic field components are shown in Fig 2

The Declination (D) at these observatories (which are all in northern hemisphere) showed positive values in the forenoon and negative values in the afternoon hours indicating southward currents in the morning and northward currents in the evening hours.

The Horizontal (H) is maximum at noon at low latitudes and minimum at high latitudes at noon suggesting eastward current at low latitudes reversing to westward current beyond the latitude of Sabhawala. The amplitude of diurnal as well as semidiurnal component shows a maximum over the dip equator.

The vertical component (Z) at all these observatories (except at Trivandrum) shows a minimum at noon characteristic of the northern hemisphere. The variation of Z and of H being similar at Trivandrum have been explained by Singh (B.P.) as due to induction effects in the subsurface geological features between India and Sri Lanka and due to currents along the Palk Strait.

These features can be represented by the equivalent overhead current system as shown in Fig 3. One finds two loops of current

Fig. 3.

system in the northern and southern hemispheres within the daytime hours. The currents in the night time are too weak to be determined by conventional magnetometers. The focus of the current systems are located at about 3.5° latitudes and at hours either close to or slightly before noon. The direction of currents loop is anticlockwise in the northern and clockwise in the southern hemisphere. The intensity of total currents, position of focus and the shape of the current loops vary with longitude, season, solar activity epochs and may be with long term secular variation effects. It is to be noted that at stations near the foci, one finds opposing currents in two directions and hence ideally there should be no variation of the horizontal field (H). At equatorial stations the effects of the northern as well of the southern loops are in the same direction and hence very large variation of the H field is observed at these latitudes.

Fig 4(a) and 4(b)

In Fig 4(a) and (b) are shown the daily variations of D, H and Z at stations near the current foci

in Indian longitudes. It is seen that the H field has significant daily variation and during some seasons becomes almost semi-diurnal in character. These features could be due to the distortions and the asymmetries in the Sq current loops.

When the daily ranges of the H field at all available observatories are plotted against latitude one obtains a curve as shown in Fig 5 a slightly modified after

Fig 5.

Onwumechilli. Instead of smooth maximum of the daily range, one finds a very narrow maximum superimposed on the smooth curve one would interpolate from the data from non equatorial latitudes. This is the characteristic of the equatorial electrojet.

The features of H and Z variations at low latitudes can be explained on the basis of a band current flowing at 105 km altitude centred over the dip equator and with very small vertical extent. The theoretically derived variations of H and Z are shown in Fig 6. One would observe a maximum

Fig 6.

of H at the dip equator, with the width of the maximum corresponding to the width of the band current. The Z variation would be zero at the centre and maxima at the edge of the current sheet. The sign of Z variation would be opposite in the either side of the equator.

Prof Chapman (1951) had derived the curves for the latitudinal variations of H and Z within the electroget regions on the basis of various shapes of the current profiles. Prof Onwumechilli has worked extensively on the modelling of the current profiles to fit the observed ground and satellite magnetic field data. Theoretical modelling has been done by Sugiura and Poros, Richmond and Untied and many other scientists.

Fig 6.

shows the position of some of the equatorial geomagnetic observatories. Note that all of these are located in DEVELOPING COUNTRIES. The difference between the geomagnetic equator (dipole, and the dip equator is the largest in West African regions pointing to special significance of geomagnetic research in the region.

Fig 8

shows the latitudinal cross section of ΔH and ΔZ across the dip equator in CHAD based on the network of nine observatories operated for some time by the French scientists

This is the only example of N-S survey of geomagnetic field across the equator ever attempted.

Fig 8.

shows the comparison of ~~rocket borne~~ the vertical profile of the current density in the electrojet by rocket borne proton precession magnetometer compared with the theoretical expectation. Note the discrepancies, the theory predicts maximum ~~large~~ current at 100 km whereas all rocket experiments observe the maximum of current at 106-107 km.

Fig 9.

Note the height of the maximum current density at 100 km and half-width of about 250 km.

Fig 10

Latitudinal cross section of daily range of H in Ethiopia on some individual days based on the array of magnetometer operated in the region

Fig 11

(a) the amplitude of sudden commencement of magnetic storms shows an enhancement over the dip equator during the daytime and the enhancement is stronger in American than in Indian zone.

(b) The amplitude of magnetic crochet (S$_q$) show enhancement at the equator, these being stronger in American than in Indian zone.

(c) In American zone the enhancement is largest at noon but significantly greater than one even at night during very high solar activity period.

Fig 12

shows the enhancement of sudden impulse over the dip equator based on the Ethiopian chain of magnetometers

Fig 13

Two examples of SSC*, sudden commencement magnetic storm in which first impulse is negative followed by the main positive impulse. These events are seen at low latitudes only between 08 - 16 local hours and only within regions few degrees from the equator. These are not seen at tropical latitudes.

Fig 14

Comparison between latitudinal variations of ΔH and the critical frequency of E_s layer ($f_0 E_s$). A close similarity suggests that E_s at low latitudes is associated with the equatorial electrojet.

Fig 15

Temporal variation in $f E_s > 5$ MHz at few typical stations. At auroral regions E_s occurs mainly at night independent of season. At north and south temperate zone E_s is most frequent during local summer day time. At

At equatorial stations E_s occurs during the daytime independant of season.

Fig. 16.

Temporal variation of occurrence of $f_{Es} > 5$ MHz at few stations in African zone. Note equatorial type of E_s is observed at Ibadan (Geom lat 11°N) and Djibouti (Geom lat 7°N) and not at Lecpoldville (Geom lat 3°S) or at Luiro (Geom lat 4°S) If one considers actual dip latitude the discrepancies are resolved suggesting the close control of ground magnetic fields even at ionospheric heights.

Fig 17

shows the starting and ending of equatorial E_s in correspondence with the period when the geomagnetic field H is above the night time level.

Fig 18

Example of an equatorial q type of sporadic E reflections on an equatorial ionogram

Fig 19

Deformation of E_s-q observed at low latitude equatorial electrojet stations

Fig. 20

Showing that the disappearance of E_s-q are associated with the decrease of H and Z components of the magnetic field.

Fig 21

Note the ionospheric drift at an equatorial station during the daytime is towards West corresponding to the electric current being Eastward

Fig. 22

Comparisons between the daily variations of ΔH and E, F region drifts at an electrojet station showing very close association of ionospheric drift with electrojet current

Fig 23.

The narrow region of the increased spread and axial ratio of ionospheric irregularities over the equator suggest their association with electrojet.

Fig. 24.

Note the gradual shift in the peak of electrojet occurring at 1040 hr local during low sunspot years to 1210 hr local during maximum sunspot years. This is due to increasing control of the electron density in the E region on the electrojet current with increasing sunspots

Fig 25

Plan of VHF forward experiment conducted in Peru during IGY period. Note the circuit Trujillo to Arequipa was associated with the scatter from the equatorial electrojet region over Huancayo.

Fig 26.

Note that the strongest signals were recorded during the daytime irrespective of the season suggesting association with equatorial electrojet

Fig. 27

Comparisons of the temporal variations of ΔH at Huancayo with the signal strength and fading rate of VHF forward scatter along Arequipa → Trujillo path. Note the absence of VHF signals during large decreases of ΔH.

Fig 28.

The ionospheric drift measurements are solely due to phenomenon occurring in the electrojet layer and hence the data can be used unlike the ground geomagnetic field for studies related to electrojet during disturbed conditions. Note the decrease of ionospheric drift and hence the electric field with increasing Kp index.

Also decrease of decreasing drift velocities with increasing B_z component of the interplanetary magnetic field.

Fig. 29.

Note the occurrence of afternoon depressions of the H field at equatorial stations

Fig 30

Fig 31

Fig. 32

Fig 33

Fig 34

Note the counter electrojet are most common around 08 hr or 16 hr local time

Fig 35

Note the counter electrojet are more frequent at any station during minimum than maximum sunspot years. Further these events are more frequent at Kodaikanal than at Huancayo. These facts suggest anti correlation between the frequency of occurrence of counter electrojets and of electrojet current strength

Fig 36.

Note two types of counter electrojet one moving with the sun along the longitude and other occurring at same UT at all stations

Fig 37

Magnetograms at two equatorial stations seperated by 2 hours in longitude and two stations in the same longitude seperated by about 10° latitude. This enables identification of solar time associated and storm time associated counter electrojet events

Fig 38

Note morning or afternoon counter electrojet are more frequent at lunar times about 2 hr.

Fig 39

First examples of the associations between depressions in ΔH, reversal of ionospheric drifts and the disappearance of equatorial Es

Fig 40

Excellent example of the disappearance of Es-q exactly when ΔH decreased below its night level and Es-q reappeared when ΔH again increased above its night level.

Fig 41

Example of frequent disappearances and appearances of Es-q during geomagnetic storms.

Fig. 42

Disappearance of Es-q and appearance of Es-f associated with counter electrojet event

Fig. 43.

Sudden disappearance or appearance of Es-q with a time period of one minute.

Fig 44.

Rocket borne instruments giving data suggesting the Es-q to be generated as a consequence of cross field instability

Fig 45.

Rocket data showing disappearance of cross field instability during counter electrojet

Fig 46

VHF backscatter, F region vertical drifts compared with ΔH and fEs-q during severe geomagnetic storms.

Fig 47.

Solar flare effects during counter electrojet event.

Fig 48.

Solar flare effect during a counter electrojet event showing negative excursion within limited latitude and longitude region

Fig 49

Effect of counter electrojet on the F region of the ionosphere, decreasing the height of the F_2 region in synchronism with ΔH.

Fig 50.

The Es-q disappears not when ΔH is below the night level but when the S_R variation across the dip equator shows a minimum at the equator.

Fig 51

Disappearance of Es-q when ΔH at equator shows a minimum but the minimum value is significantly positive

Fig 52

Disappearance of VHF radar echoes from the E region during the negative values of ΔH equatorial minus ΔH at non electrojet stations on the same longitude.

Fig 53.

Relation between VHF backscatter doppler shift and ΔH at low latitude stations. Note better correlation when ΔH equatorial minus ΔH non equatorial station is used to define equatorial electrojet strength.

Fig 54.
Relationship between VHF ft backscatter doppler shift and ΔH during disturbed conditions

Fig 55

Fig 56.
(a) Note sudden reversals of E and F region drifts at Jicamarca coincident with the reversal of IMF from southward to northward directions at 0345 LT on 3 July 1968.
(b) Note sudden decrease of E and F region drifts coincident with sudden decrease of ΔH ~~at~~ in the afternoon hours associated with northward turning of the IMF.

Fig 57
An example showing the decrease in ΔH at Huancayo coincident with northward turning of IMF

Fig 58
Comparison between the fluctuations of equatorial electrojet current at different longitudes and the fluctuations of IMF

Fig 59.
Correlation between changes in Bz and electrojet current

Fig 60
A compressed state of magnetosphere is more favourable to produce a ~~little~~ big changes in electrojet due to fluctuations in θ of IMF.

Fig 61
A large fluctuation train in ΔH at Huancayo at Thule and of IMF latitude.

Fig 62
An example showing close relationship between the fluctuations of the electric field in the night side of the equatorial region with the fluctuations in the electrojet in the dayside.

Fig 63
Simultaneous fluctuations in the magnetic fields at equatorial and polar latitudes

Fig 64
Example showing changes in electrojet current associated with sudden commencement of geomagnetic storms

Fig 65.
A close correlation between changes in ΔH and the signal strength of VHF forward scatter signal during different forms of SSC.

Fig 66
Examples showing that SSC^{A} are associated with impact of solar plasma changing IMF near the magnetopause from south to north direction

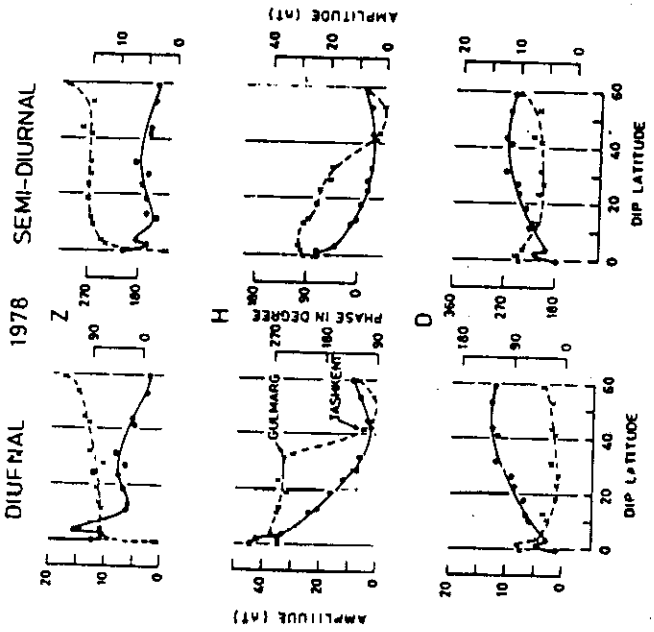

~~Figure 3~~. Latitudinal variations of the amplitude (solid line) and phase (broken line) of the diurnal and semi-diurnal terms of daily variations in the three geomagnetic components D, H and Z.

Fig. 2

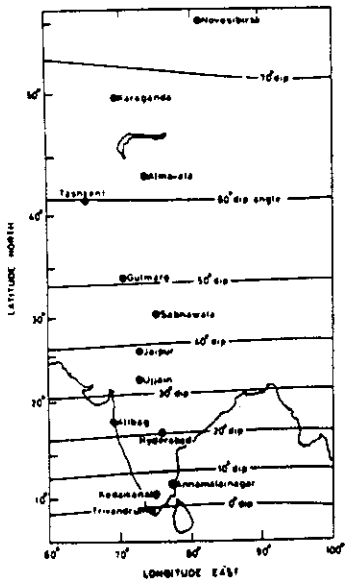

~~Figure 1~~. Map showing the locations of magnetic observatories whose data are used in the present analysis.

Fig 1(a)

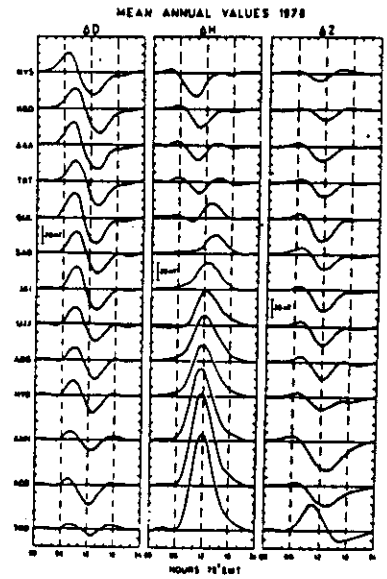

~~Figure 2~~. Solar quiet-day variations in geomagnetic field components, D, H and Z at magnetic observatories along Indian longitudinal belt for the year 1978.

Fig 1(b)

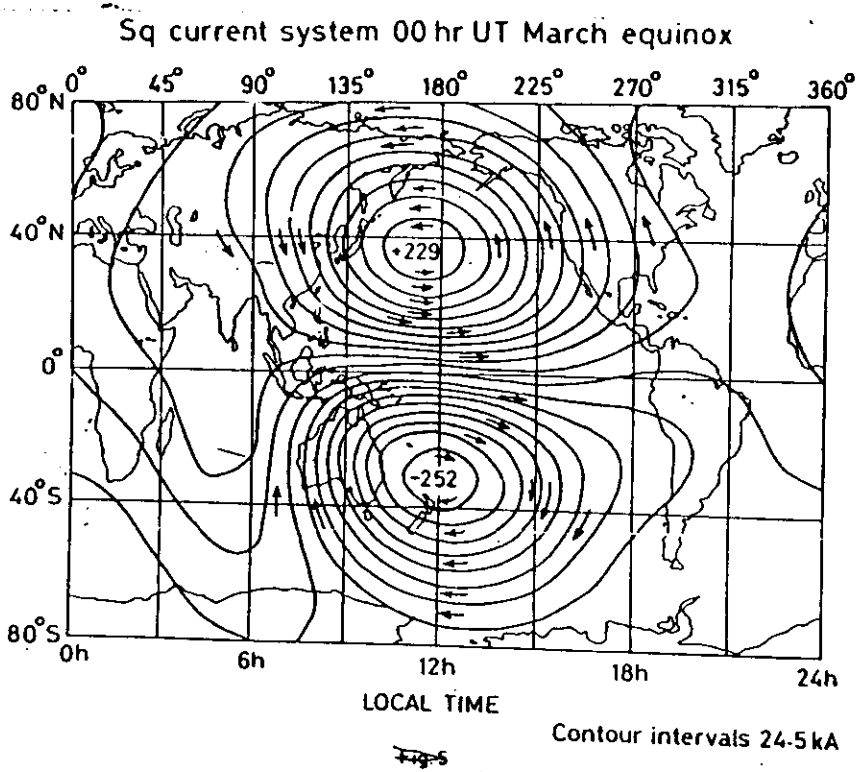

~~Fig 5~~

Fig. 3.

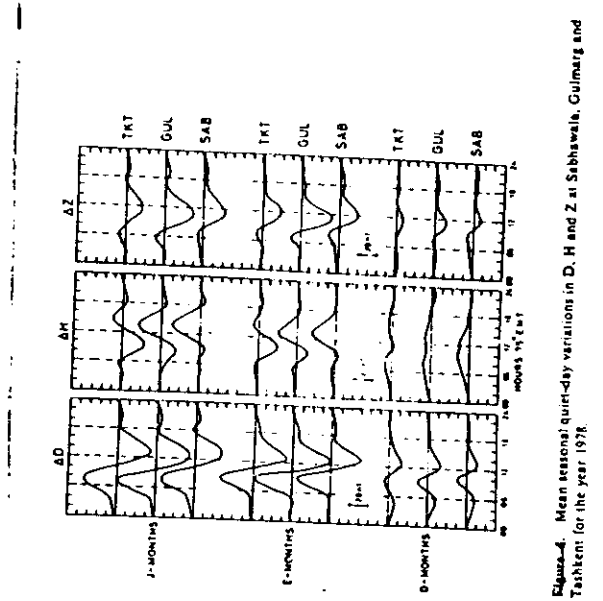

Figure 4. Mean seasonal quiet-day variations in D, H and Z at Sabhawala, Gulmarg and Tashkent for the year 1978.

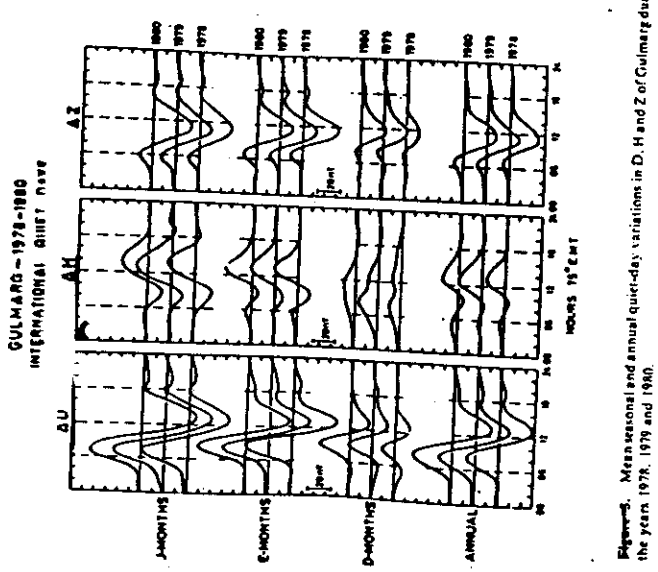

Figure 5. Mean seasonal and annual quiet-day variations in D, H and Z of Gulmarg during the years 1978, 1979 and 1980.

Fig. 4

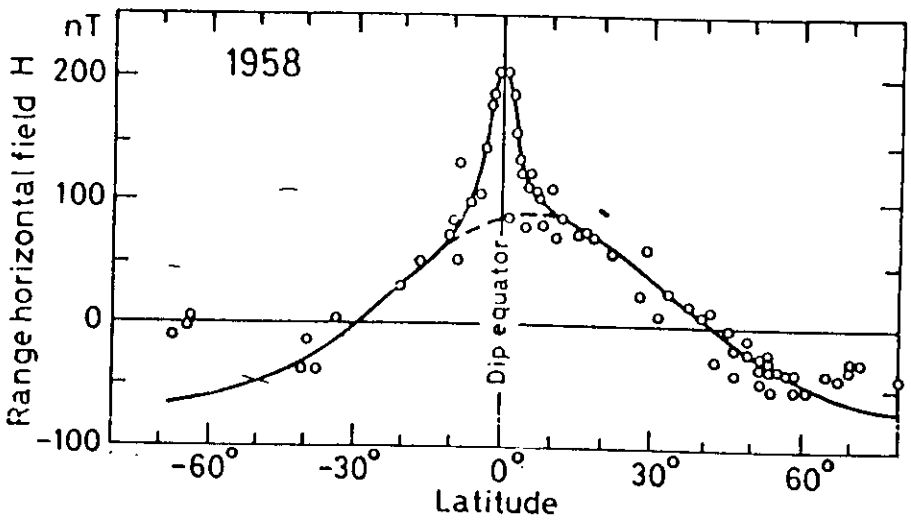

Fig. 6

Fig. 5.

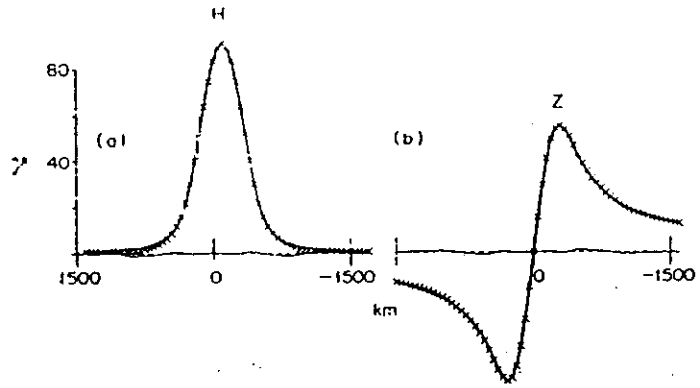

Profiles of the current distribution of the Richmond model (crosses) and profiles of the fourth-degree model (a) or parabolic model (b) which approximate the best that distribution. Profiles of residues with the same scale.

Fig. 6.

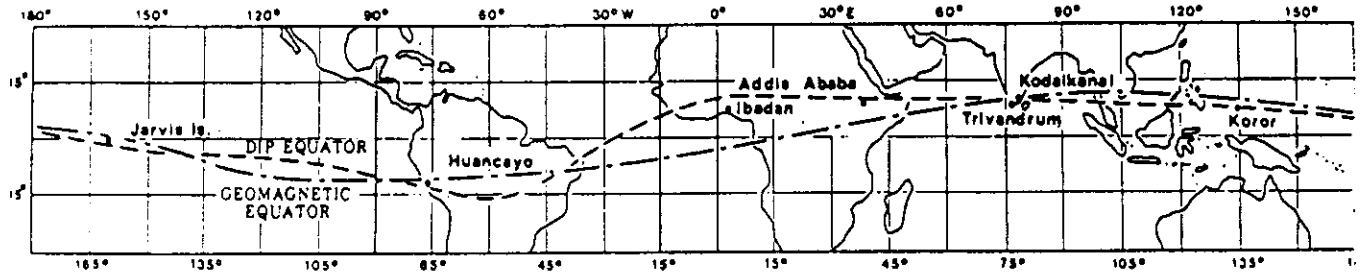

Locations of the geographic, geomagnetic, and dip equators and of several equatorial magnetic observatories. (Figure is from *Gupta* [1973*b*]. Reprinted by permission of Centre National de la Recherche Scientifique.)

Fig 7

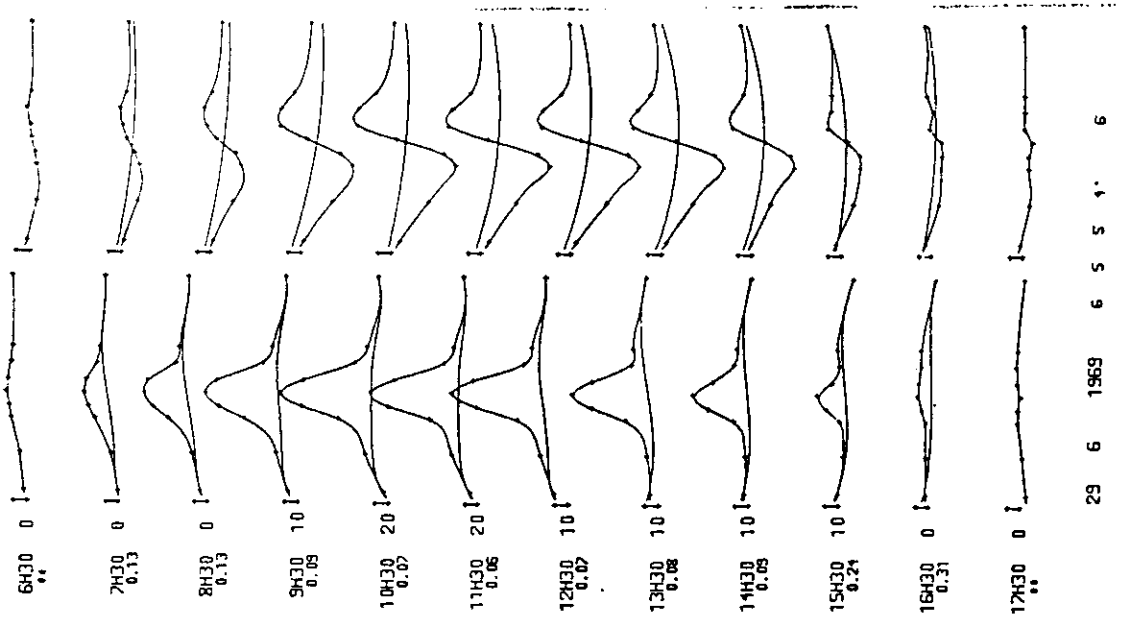

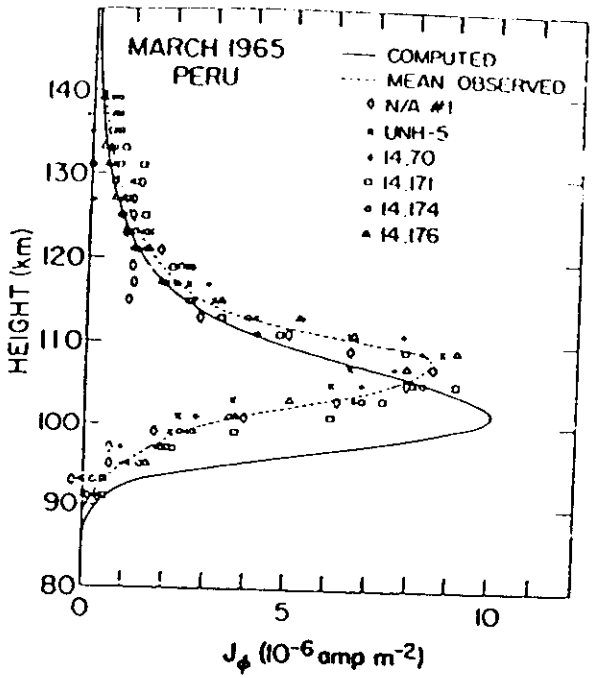

Observed and computed eastward current density profiles near noon at the dip equator off the coast of Peru in March 1965, normalized to $\Delta H = 100\ \gamma$ at Huancayo. Measured profiles are from *Shuman* [1970] (flight N/A #1), *Maynard* [1967] (flight UNH-5), and *Davis et al.* [1967] (flights 14.70, 14.171, 14.174, and 14.176). The theoretical profile is from *Richmond's* [1973*a*] theory (Figure is from *Richmond* [1973*b*]. Reprinted by permission of Pergamon Press.)

Fig. 8

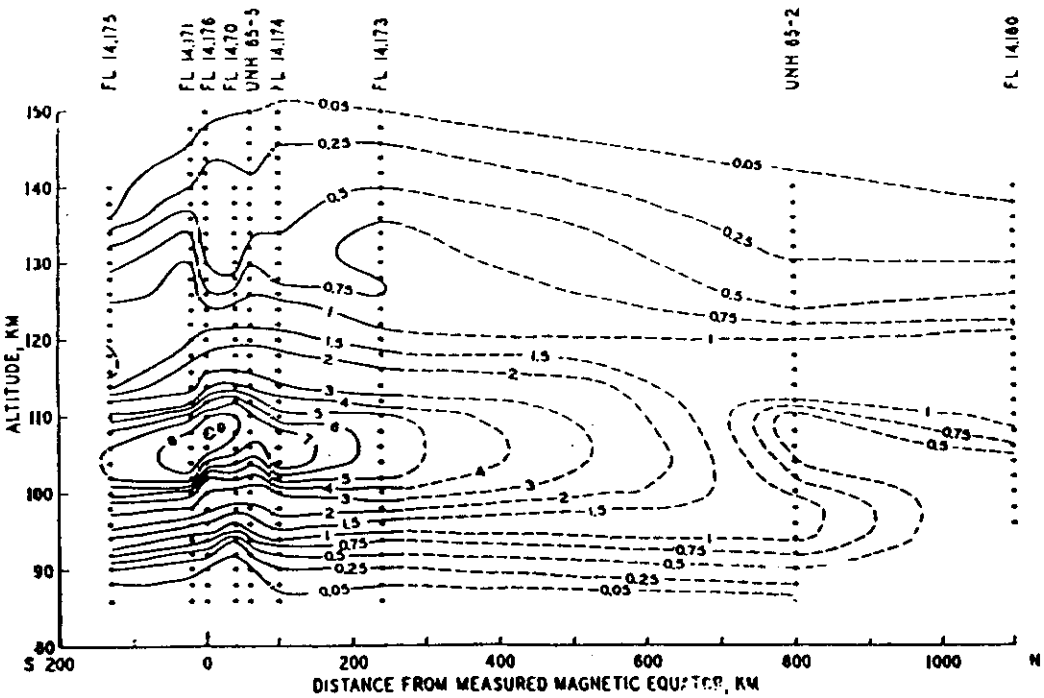

Cross-sections. profile of the equatorial electroject obtained from nine rocket flights off the coast of Peru in 1965, normalized to yield $\Delta H = 100\ \gamma$ at Huancayo. Circles indicate locations of data points used to obtain the contours of current density in microamps per square meter. The right-hand portions of the contours are dashed to indicate uncertainty associated with the relative lack of data for this portion of the diagram. (Figure is from *Davis et al.* [1967].)

Fig. 9

(a)

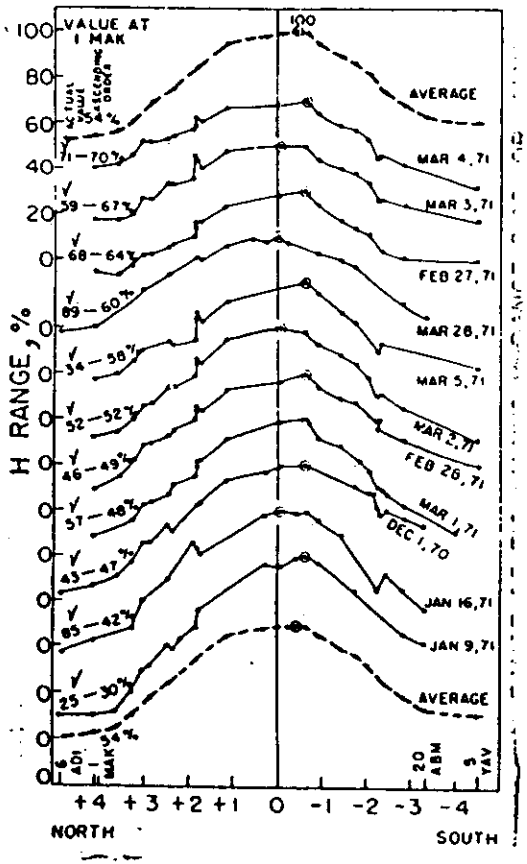

Fig. 10

R.G. Rastogi et al.,
JATP 1964, Vol. 26
pp. 771.

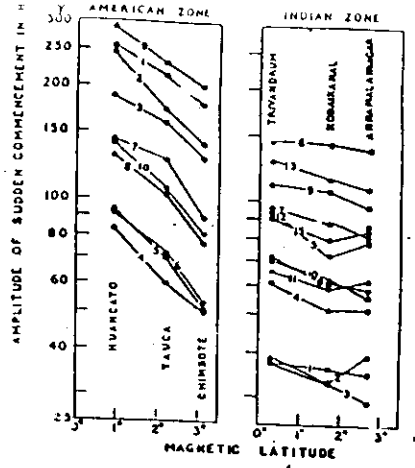

The variations with magnetic latitude of the SC in H between 1000–1400 hours L.M.T. during I.G.Y. and I.G.C. at American and Indian stations. The numbers on the lines joining the points refer to the serial numbers of the SC in

Rastogi R.G. et. al.,
JATP, 1965, Vol. 27
pp. 663

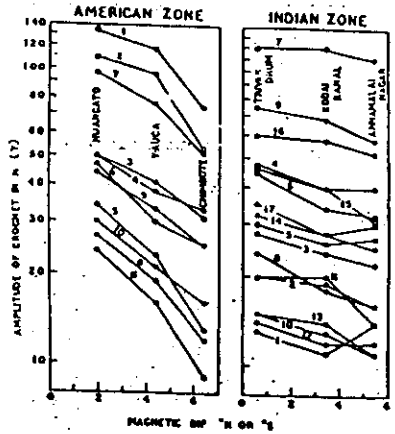

Letitudinal variation of the amplitude of solar flare crochets around local mid-day hours.

Rastogi R.G. et. al.
JATP, 1966, Vol. 28,
pp. 303

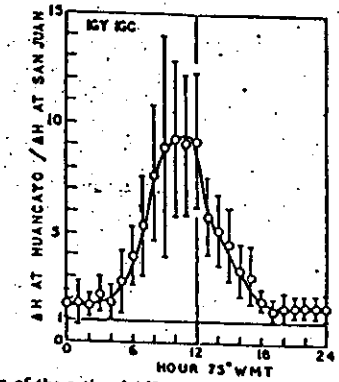

Variation of the ratio of ΔH at Huancayo to the same at San Juan at different times of the day

Fig. 11

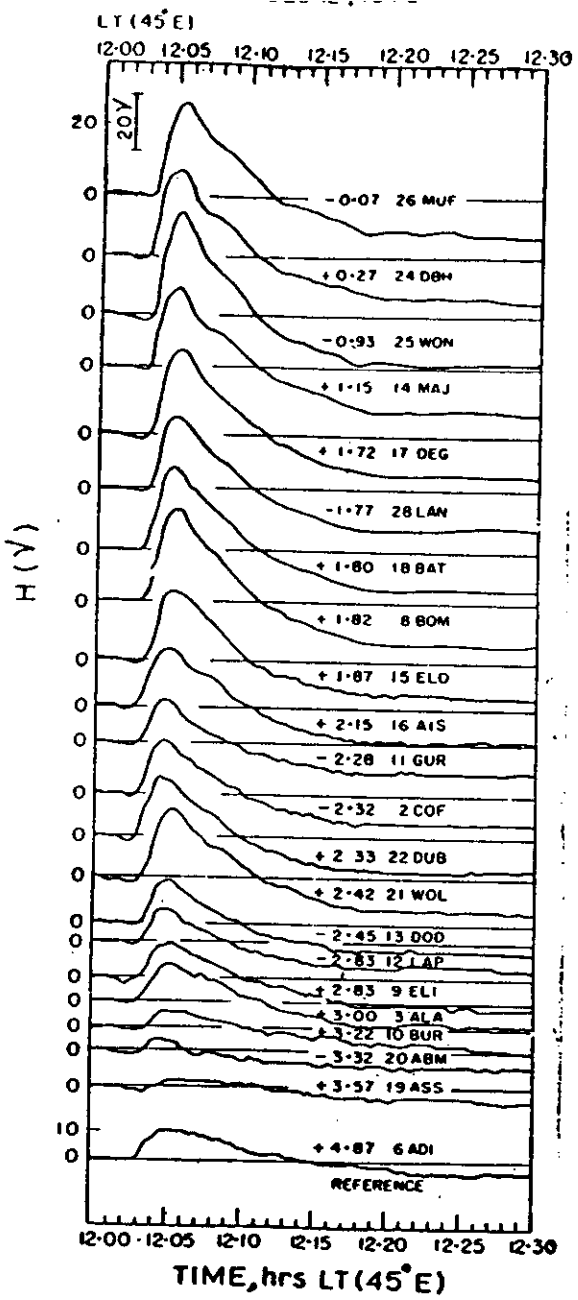

The sudden impulse (SI) in *H* on 12 Dec. 1970 at 1203 hrs ET (45°)

Fig 12

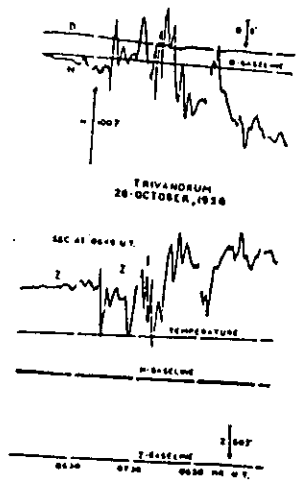

The magnetogram tracing on 28 October 1958 at Trivandrum showing SC−+ event in all the three components of the geomagnetic field.

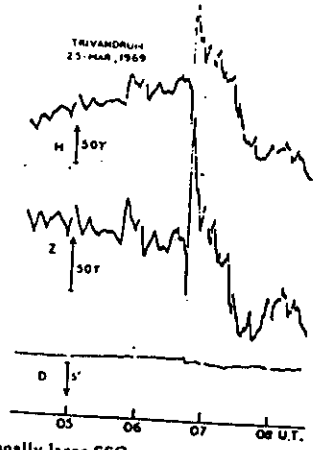

An exceptionally large SSC−+ event in all the three components of geomagnetic field recorded at Tirvandrum on 25 March 1969.

Rastogi R.G. and N.S. Sastri J. Geomag. Geoelectr., 26, 529-537, 1974 p. 529

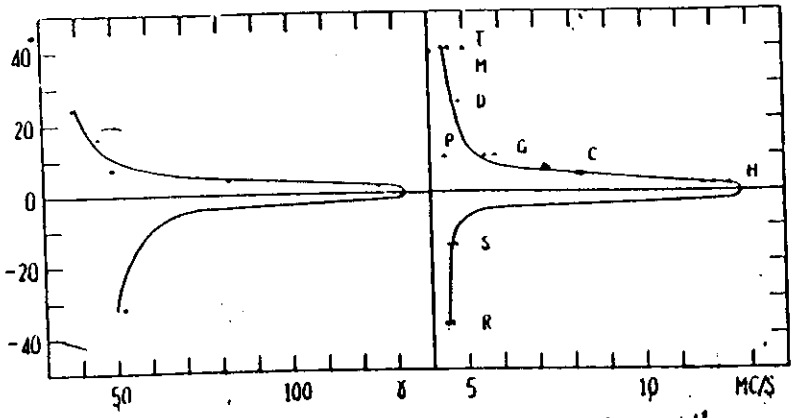

Fig. 3 Distribution of ranges of daily variation of the horizontal magnetic force (left part – after J. Egedal) and distribution of f_{Es} in the day-time (right part), near the magnetic equator. Names of stations are shown in Fig. 1. Ordinate: magnetic dip.

▼ : March 1946) (only at Christmas Island for reference)
■ : April 1946)
● : September 1949 ◆ : October 1949 × : March 1950

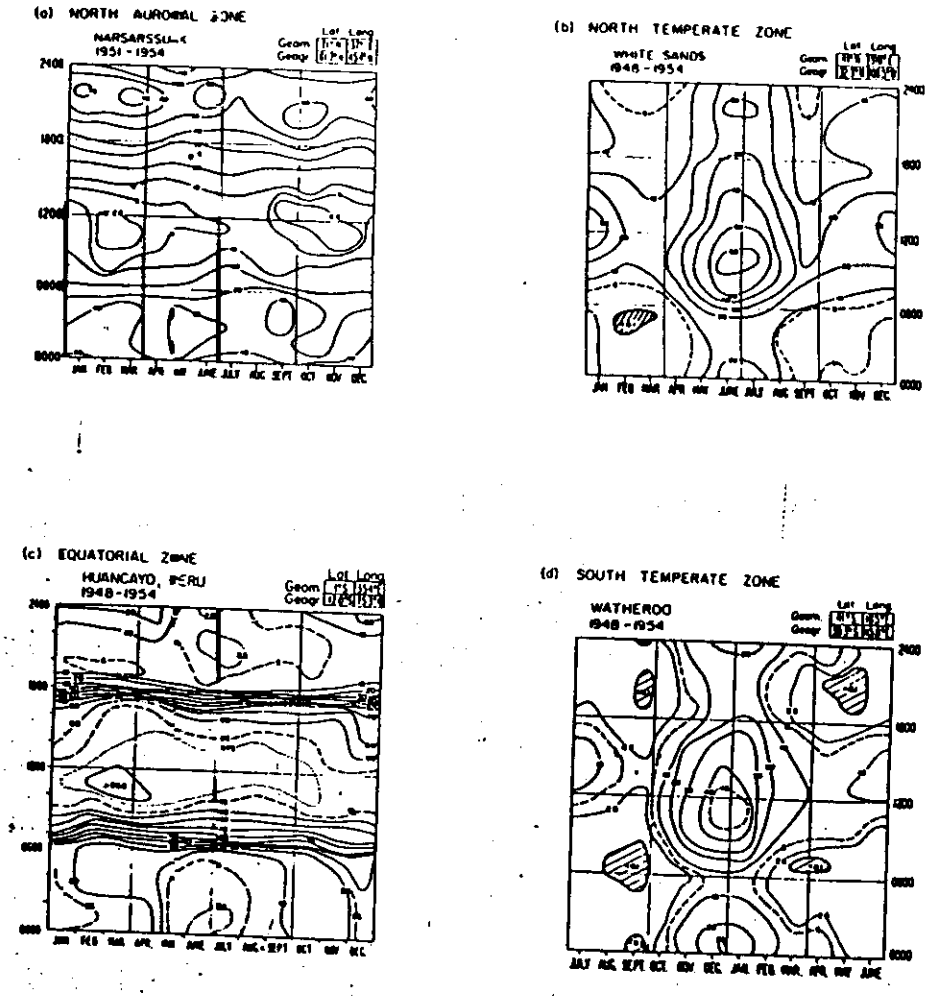

Fig. 1 Sample temporal variation in Es in terms of percentage of time for which fEs exceeds 5 Mc/s

Fig 15

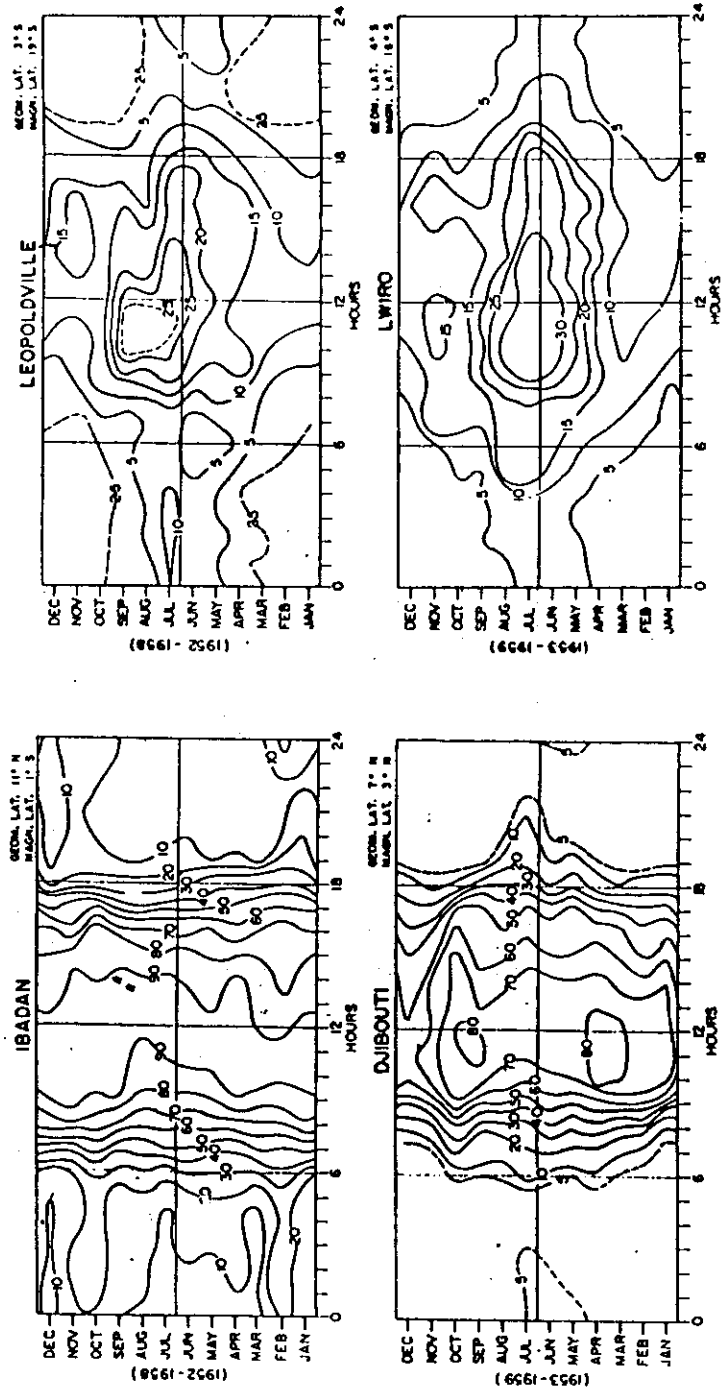

were magnetically quiet, the A_p value being 4 on the 20th and 5 on the 23rd. At none of the three hourly intervals on these days did the K_p figure reach even 3. The symmetrical ring current effect on these days, according to Sugiura and Cain (1970), was not more than 15 γ. Thus it is reasonable to assume that the geomagnetic field changes on these days, were primarily due to currents flowing in the ionospheric dynamo region.

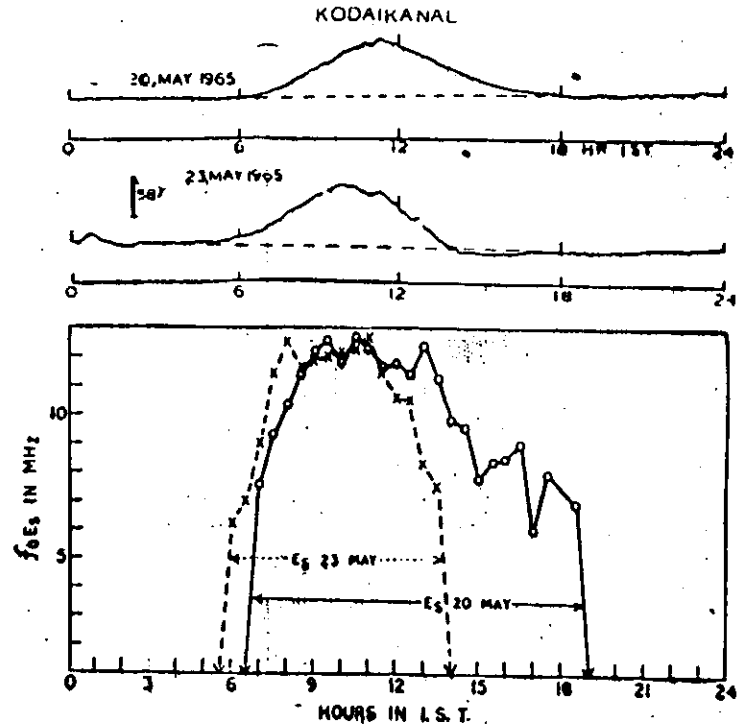

FIG. 3. Daily variations of f_0E_s at Kodaikanal on two magnetically quiet days with different periods of duration of the eastward equatorial electrojet current.

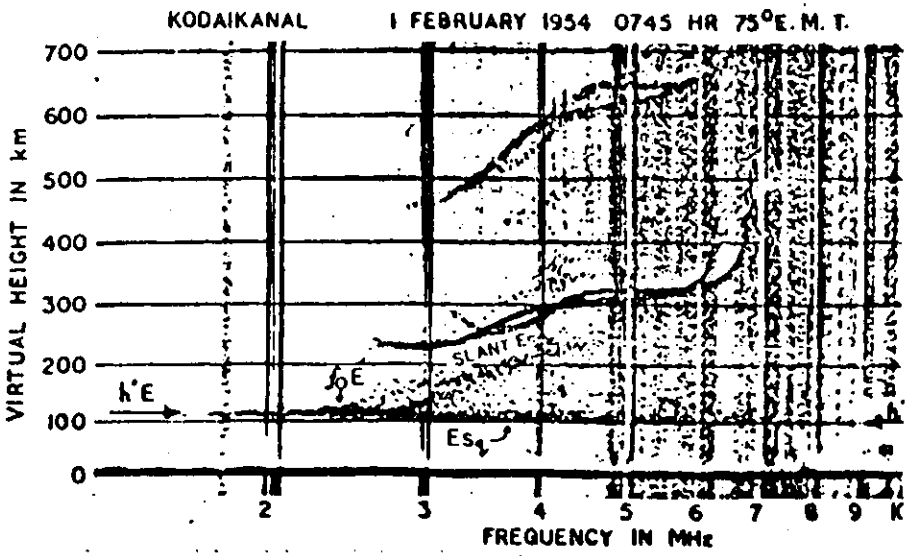

Typical day-time ionogram at Kodaikanal showing the normal E-region as well as the equatorial (q) at types of sporadic E reflections

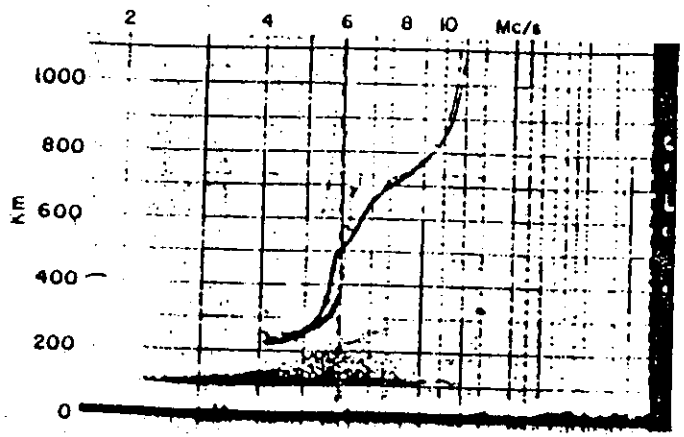

EQUATORIAL Es AT HUANCAYO
1530 DEC. 29, 1957

E_s) at Huancayo is shown on the ionogram reproduced as Fig. 1. The characteristics of E_{s-q} are given below.

(a) It regularly occurs during the daylight hours in a narrow belt along the magnetic equator.

(b) It is always partially transparent to probing radio waves; that is, it never blankets radio reflections from higher layers.

(c) It usually shows a well-defined lower edge lying between 100–110 km giving scattered and diffuse echoes above the principal echo.

(d) In well-developed cases, the diffuse echoes are contained below a sharp upper boundary that starts at about f_0E and increases in height with increasing frequency.

(e) The maximum frequency returned, (f_0E_s), usually ranges from 8 to 13 Mc/s primarily depending on the proximity of the ionosonde to the magnetic equator.

(f) Multiple echoes are not observed.

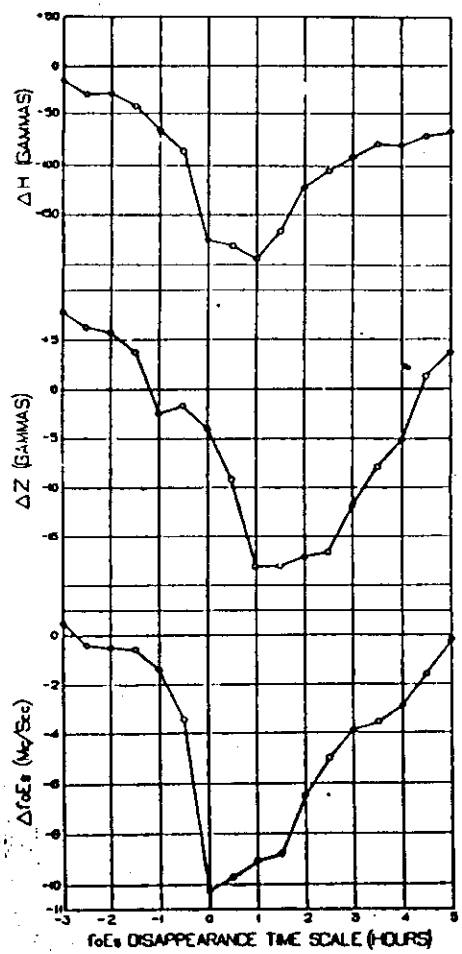

Fig. 2. Departures in H and Z components of earth's magnetic field with those

Fig. 20

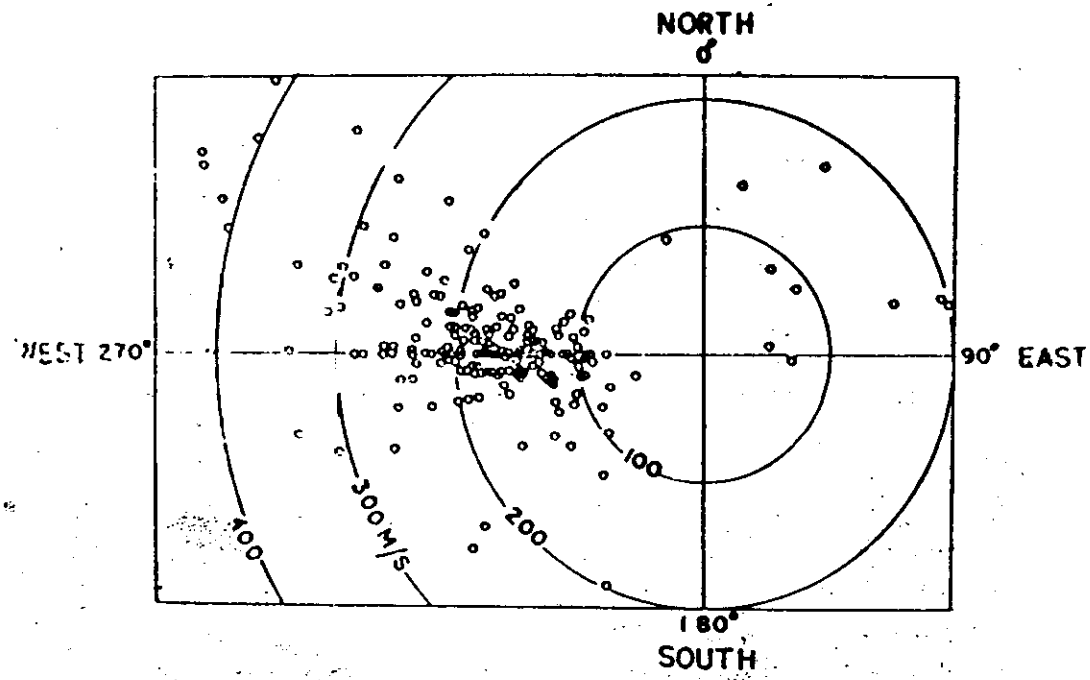

Fig. 1 : Vector plot of the E-region drift speed at Thumba during daytime hours of Jan–Feb 1964 (after Rastogi et al 1972).

Fig 21

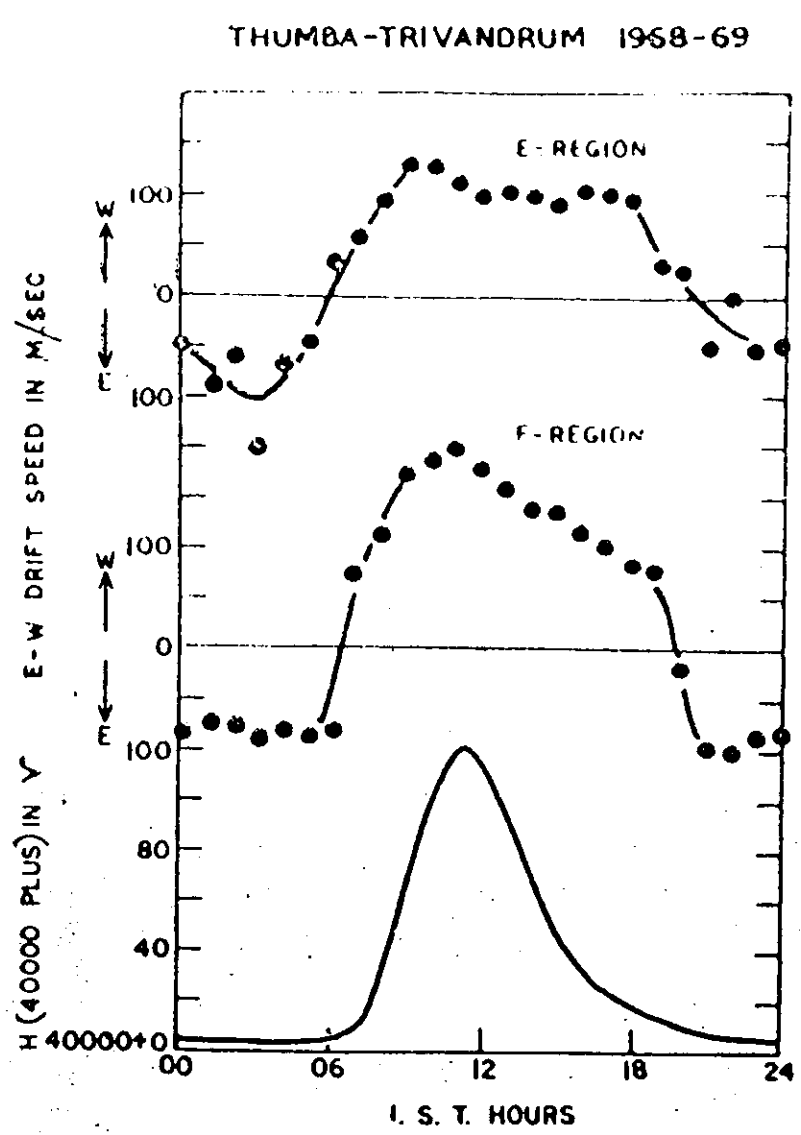

Fig. 2: Annual meas daily variations of the E and F region eastward drift velocity (Thumba) and the geomagnetic H component (Trivandrum) averaged for the period 1968-69 (after Rastogi et al. 1972).

Fig. 22

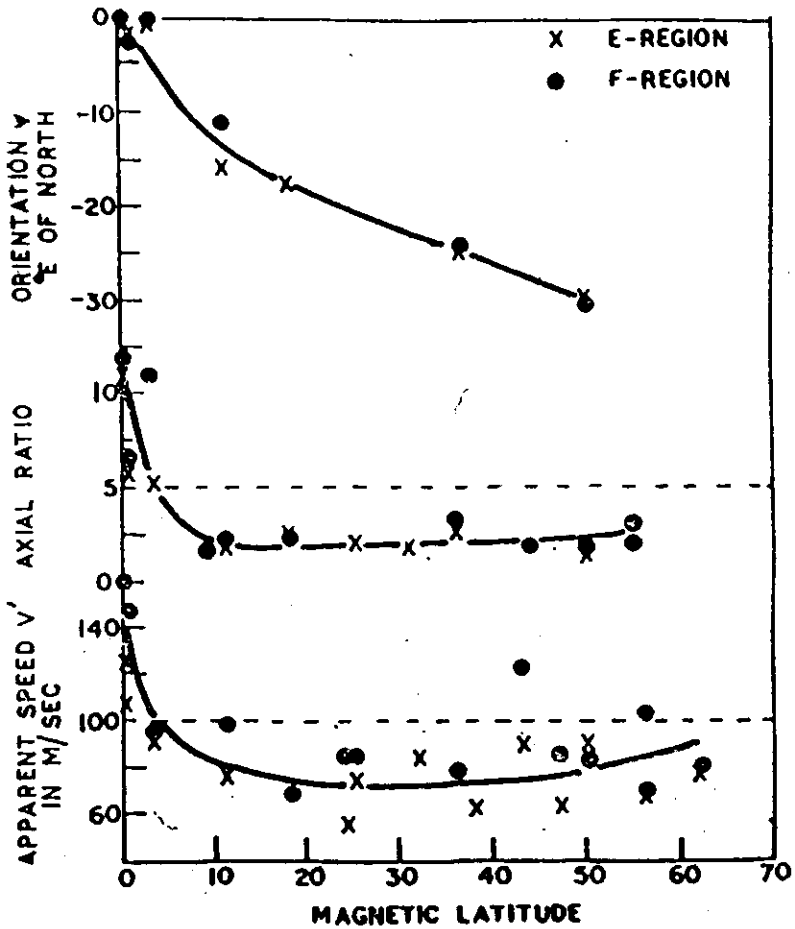

Fig. 3: Latitudinal variations of the drift speed elongation ration and the orientation of the ground diffraction patterns (after Rastogi et al. 1972).

Fig. 23

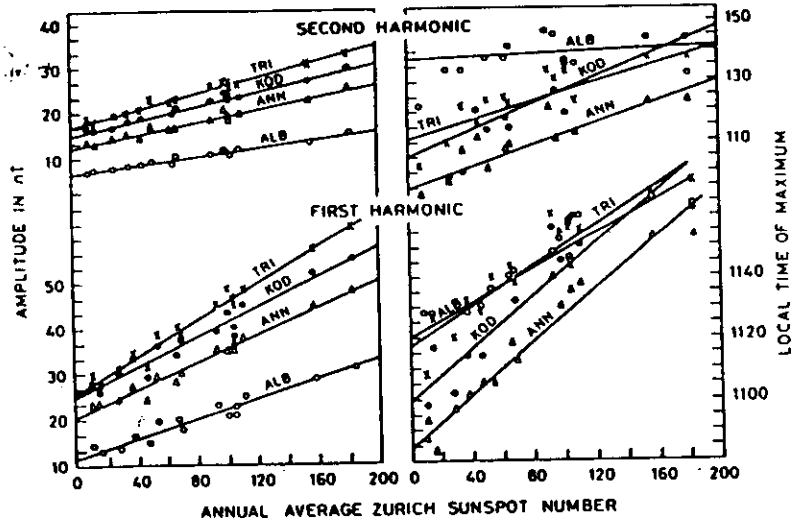

Fig. 9. Amplitudes and phases of the diurnal and semidiurnal components of the daily variation of H at four Indian tations as a function of annual average Zurich sunspot number. (Figure is from *Rastogi and Iyer* [1976]. Reprinted by ermission of University of Tokyo Press.)

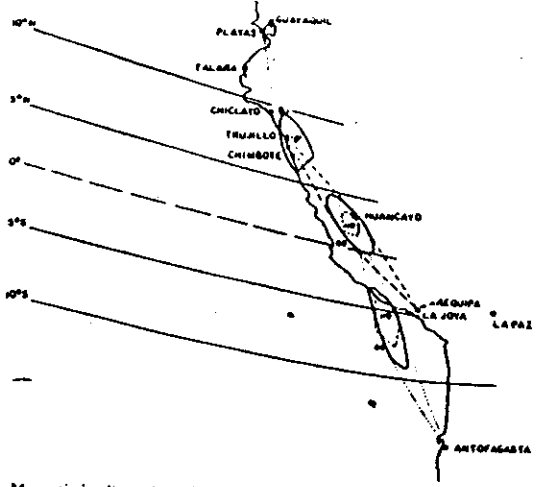

Fig. 2. Magnetic isoclines along the west coastal area of South America, with the approximate loci of antenna-beam intersections computed for the height (in kilometers) adjacent to each locus. The diagram is for three propagation paths in the E region.

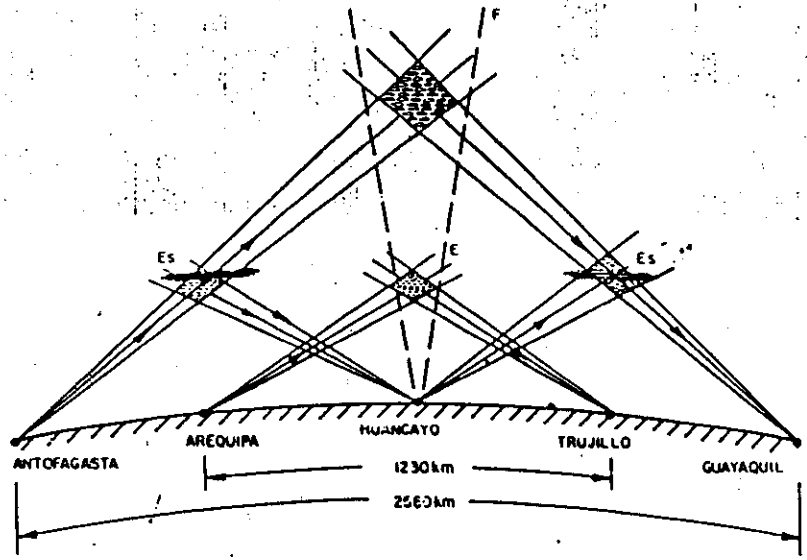

FIGURE 2. *Schematic diagram of the vertical cross sections of antenna beam intersections along the west coast of South America, indicating four of the propagation paths referred to in this paper.*

24

Fig. 25

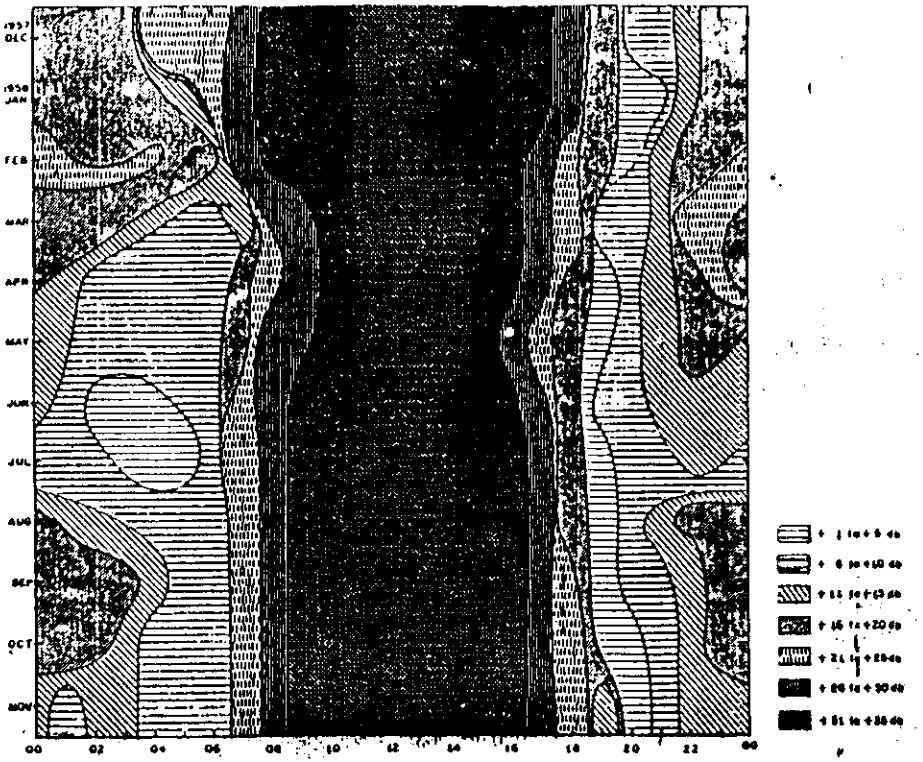

ARQ ⟶ TRU Temporal variation of the decibel level exceeded 10 % of the time

FIGURE 15. *Contours showing the temporal and seasonal variation of the range of signal strength exceeded 10 percent of the time over the central path.*

Fig. 26

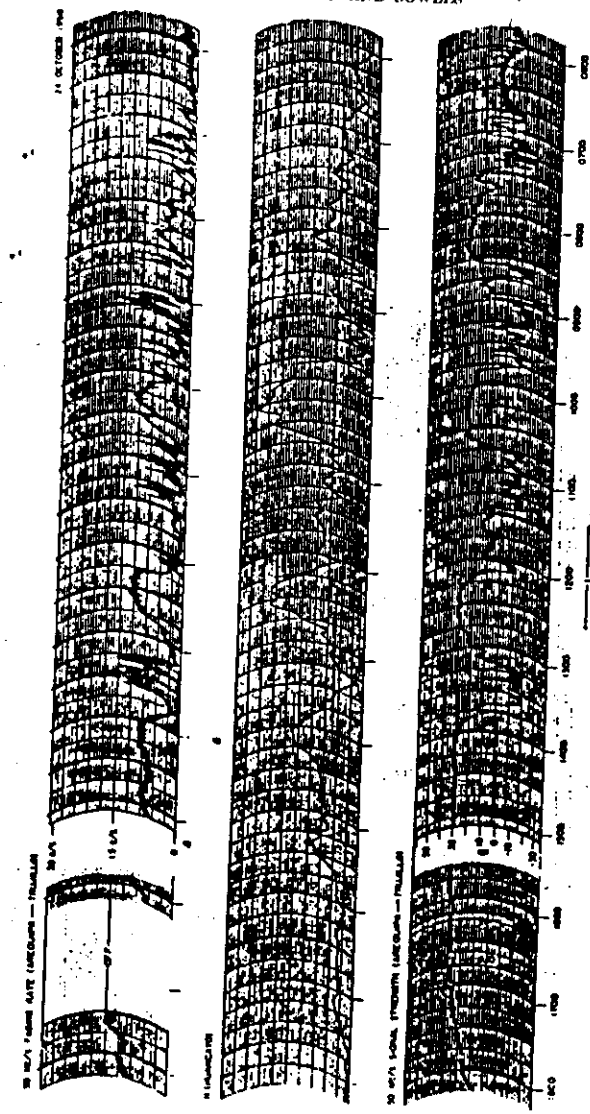

FIG. 19. A comparison for October 24, 1958, of the Huancayo horizontal magnetic intensity with the Arequipa → Trujillo signal intensity at 19.92 Mc/s and with the fading rate of that signal. The calibration of the fading-rate record indicates the instantaneous principal frequency component (in cycles per second) of the received signal intensity. The two horizontal lines added to the tracing of the Huancayo magnetogram are estimates of the apparent 'thresholds' of horizontal magnetic field strength during the periods for which they were drawn.

Fig. 27

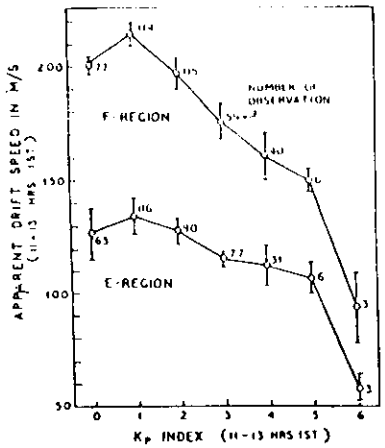

Fig. 1 The relation between apparent drift speeds in the E and F regions over Thumba and the magnetic K_p index for the year 1964.

Rastogi R.G. et al. Nature P.Sci., Vol. 233 p.13 (1971)

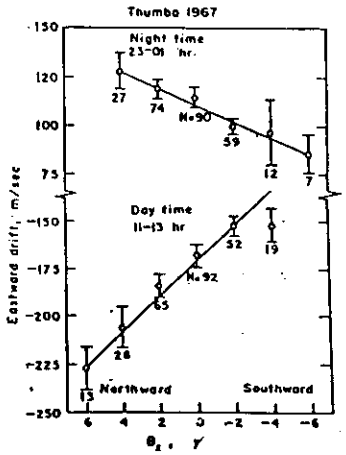

Fig. 1. Variations of the eastward component of the ionospheric F-region drift speed at Thumba during daytime (11–13 LT) and during nighttime (23–01 LT) with interplanetary magnetic field component (B_z) perpendicular to the ecliptic plane. Northward B_z is taken as positive and southward as negative.

Rastogi R.G. et al. J.A.T.P., 1974, Vol.36 p. 377

Fig. 28

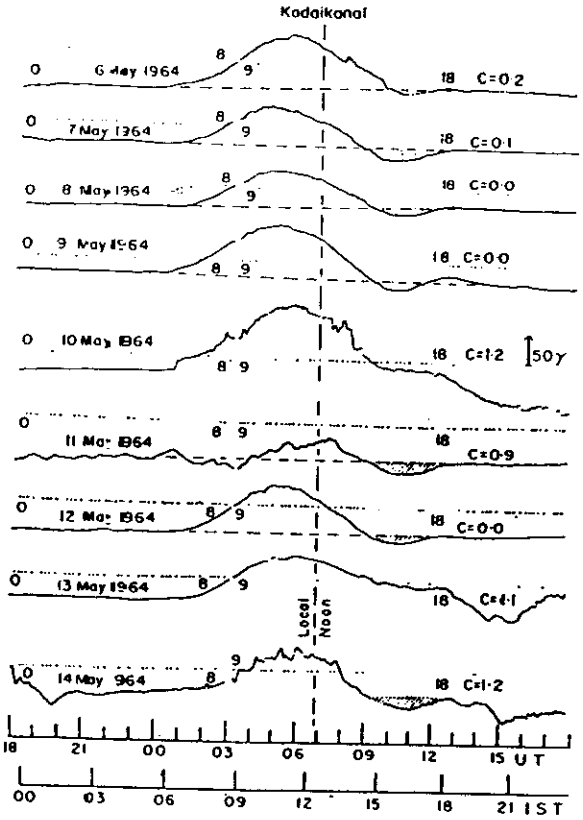

REPRODUCTION OF H MAGNETOGRAMS AT KODAIKANAL ON SERIES OF DAYS FROM 6 TO 14 MAY 1964 SHOWING THE AFTERNOON DEPRESSION OF H.
It is to be noted that on disturbed days (10 and 13 May 1964) there is no minimum in the afternoon although there is evidence of the effect around those hours.

Fig. 29

Fig

VOL. 79, NO. 10, PP. 1503–1512 JOURNAL OF GEOPHYSICAL RESEARCH APRIL 1, 1974

Westward Equatorial Electrojet During Daytime Hours

R. G. RASTOGI

Department of Physics, University of Denver, Denver, Colorado 80210

The phenomenon of the depression of the geomagnetic horizontal field during the daytime hours of magnetically quiet days at equatorial stations is described. These events are generally seen around 0800 and 1600 LT, being more frequent during the evening than the morning hours. The evening events are more frequent during periods of low solar activity and in the longitude region of weak equatorial electrojet currents. The latitudinal extent of the phenomenon is limited to the normal equatorial electrojet region, and on some occasions the phenomenon is not seen at both stations separated by only a few hours in longitude. During such an event the latitudinal profile of the geomagnetic vertical field across the equator is reversed, the ionospheric drift near the equator is reversed toward the east, the q type of sporadic E layer is completely absent, and the height of the peak ionization in the F_2 region is decreased. It is suggested that these effects are due to a narrow band of current flowing westward in the E region of the ionosphere and within the latitude region of the normal equatorial electrojet due to the reversal of the east-west electrostatic field at low latitudes.

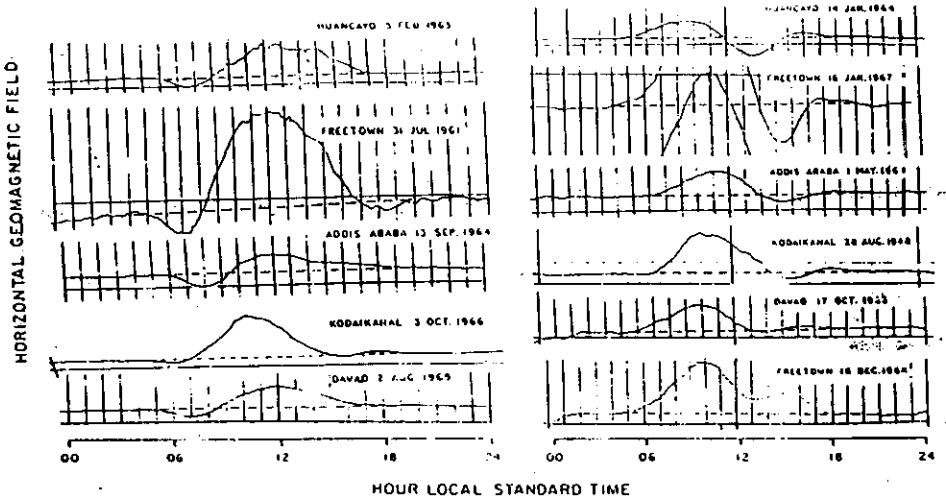

Fig. 1. Examples of daytime depressions in the H field at equatorial stations for (*a*) during the morning hours and (*b*) during the evening hours.

Fig 30

R. G. RASTOGI

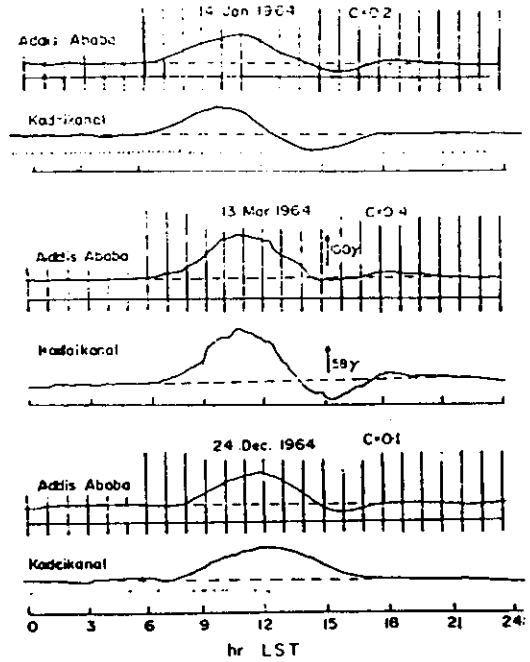

REPRODUCTION OF MAGNETOGRAMS AT ADDIS ABABA AND KODAIKANAL SHOWING THE OCCURRENCE OF AFTERNOON DEPRESSION IN H AT ONE OR BOTH THE STATIONS.

Fig. 31

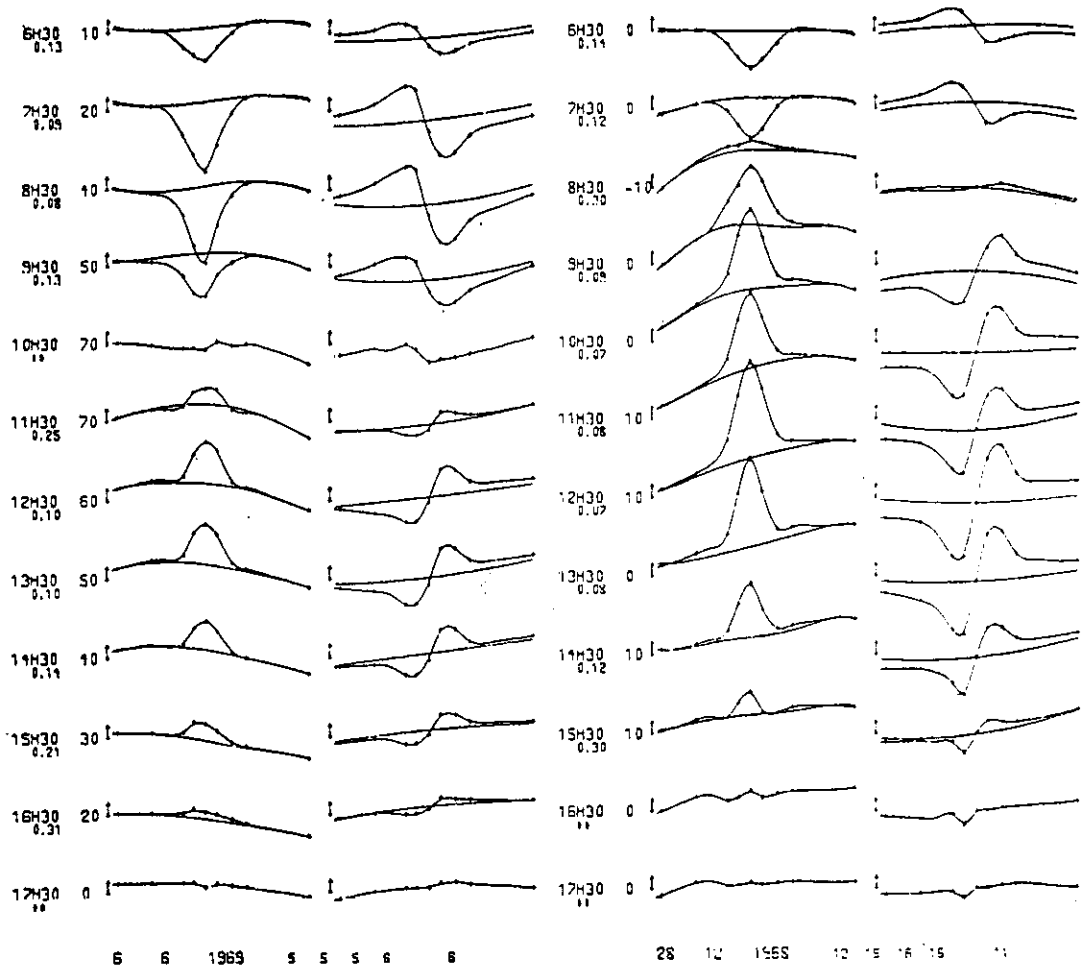

Fig. 32

Example of morning counter-electrojet at both solstices

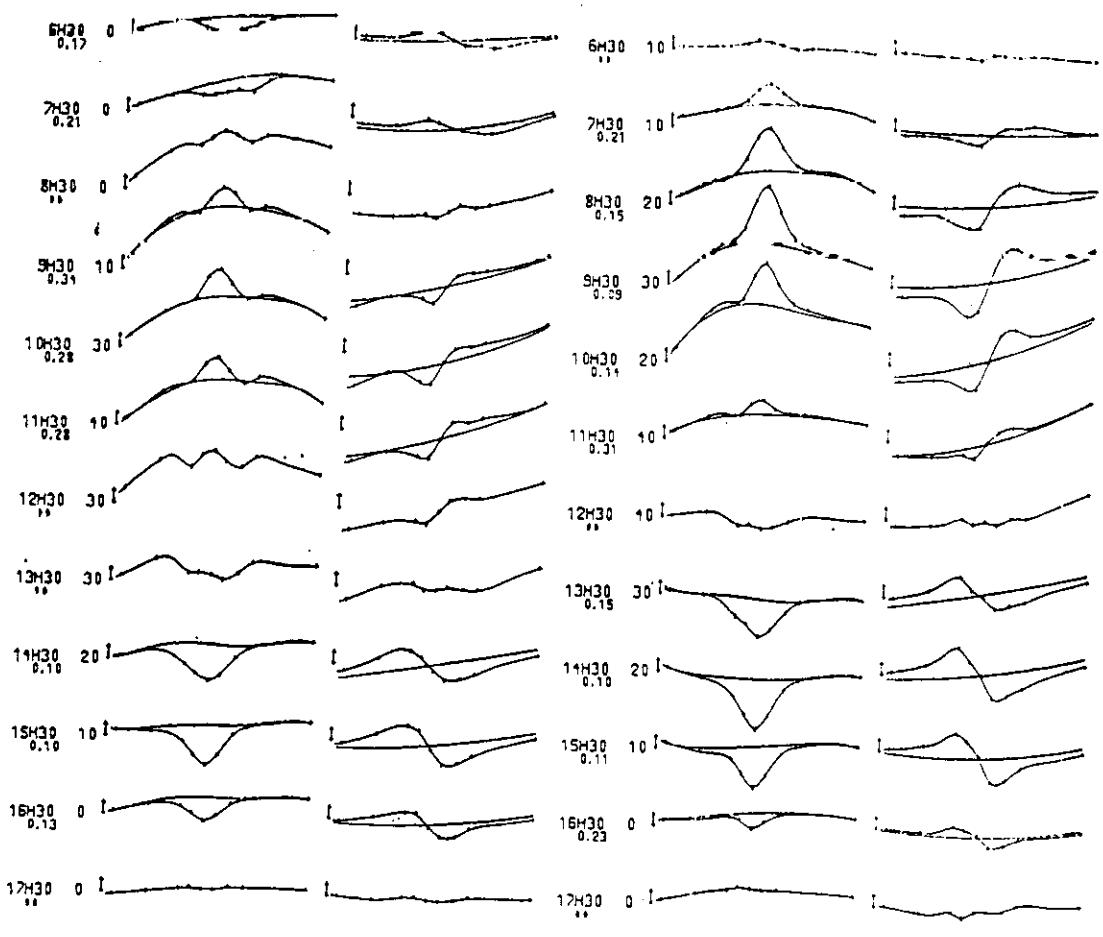

Fig. 33

Example of afternoon counter-electrojet at both solstices

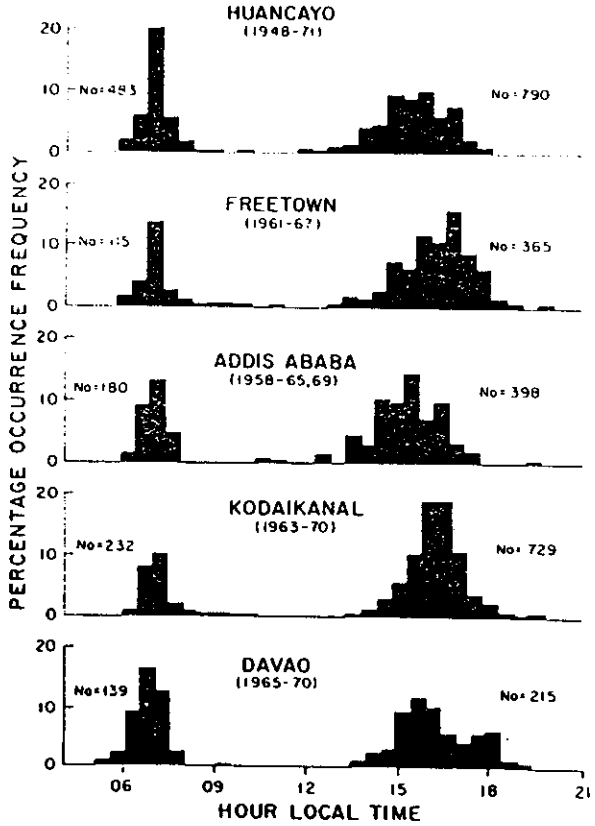

Histograms showing the percentage occurrence frequency of the daytime depression in *H* at a number of equatorial stations during the morning and the evening hours.

Fig. 34 JGR 79 1503 (1974)

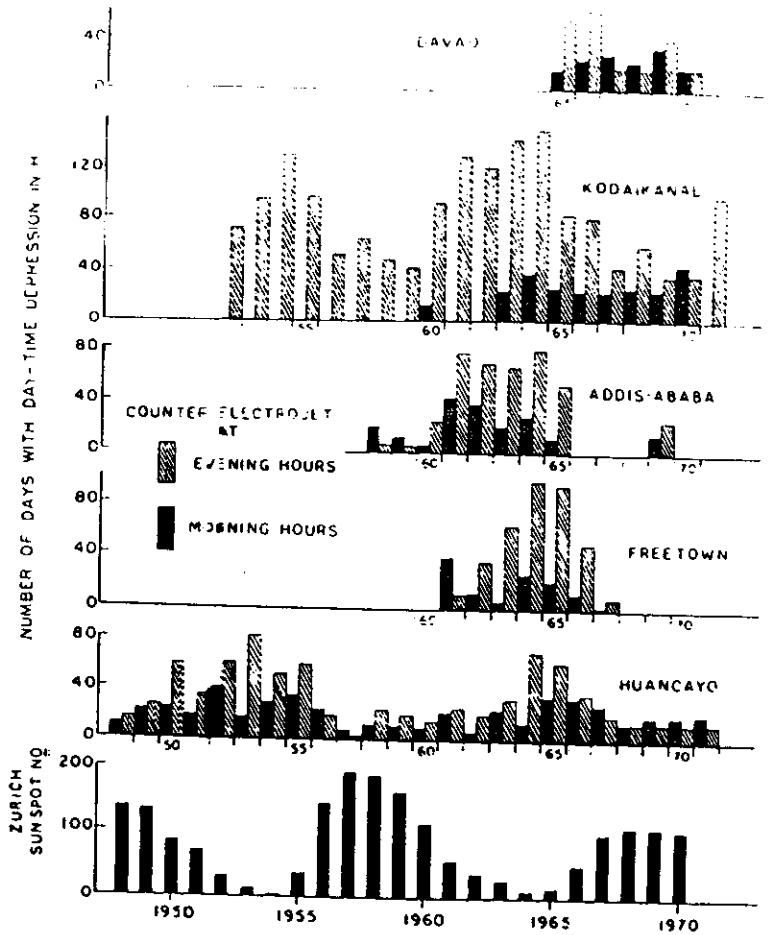

Yearly average number of depressions in the *H* field during the morning and the evening hours for different years at a number of equatorial stations.

Fig. 35 JGR 79 1503 (1974)

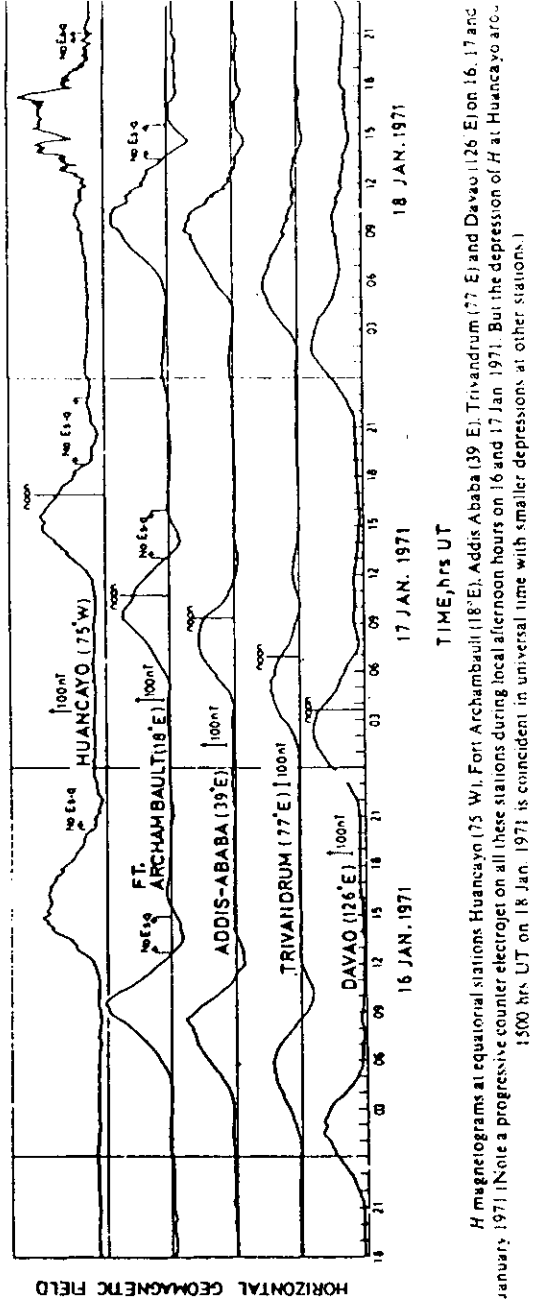

H magnetograms at equatorial stations Huancayo (75 W), Fort Archambault (18°E), Addis Ababa (39 E), Trivandrum (77 E) and Davao (126 E) on 16, 17 and January 1971 (Note a progressive counter electrojet on all these stations during local afternoon hours on 16 and 17 Jan 1971. But the depression of *H* at Huancayo around 1500 hrs UT on 18 Jan. 1971 is coincident in universal time with smaller depressions at other stations.)

Fig 36

IJRSP 10, 1 (1981)

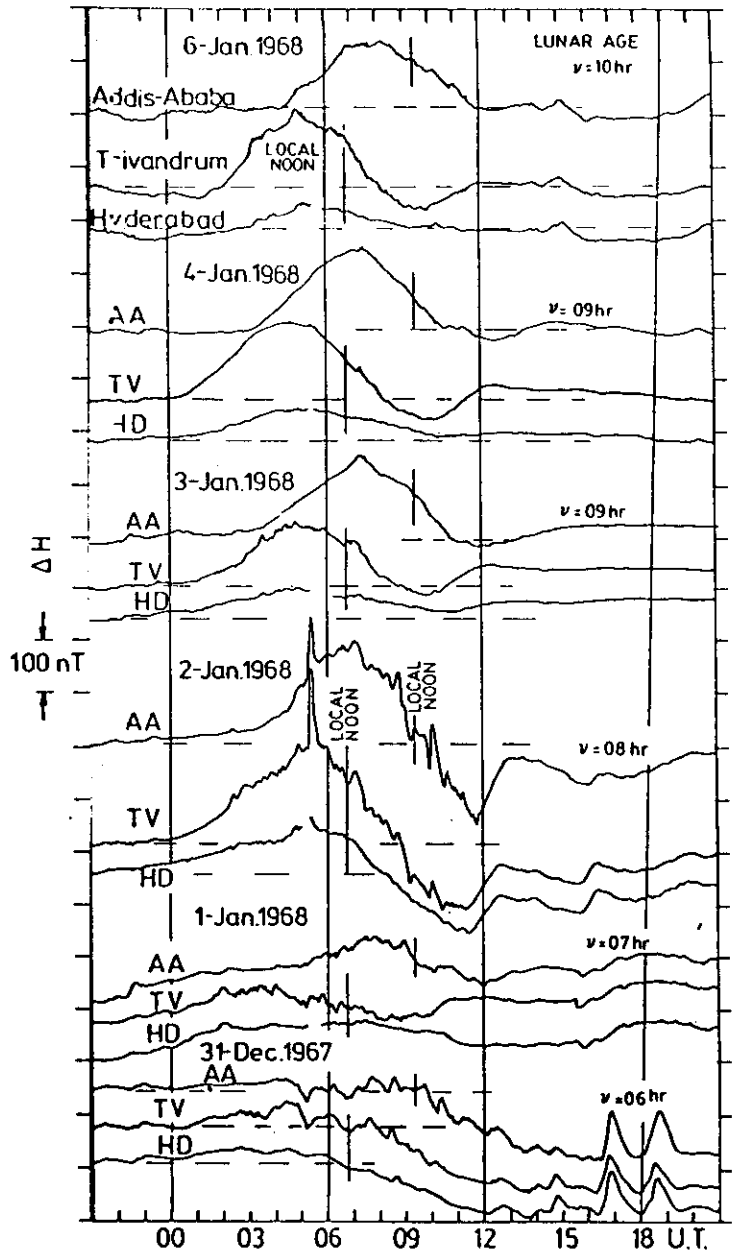

Fig. 37

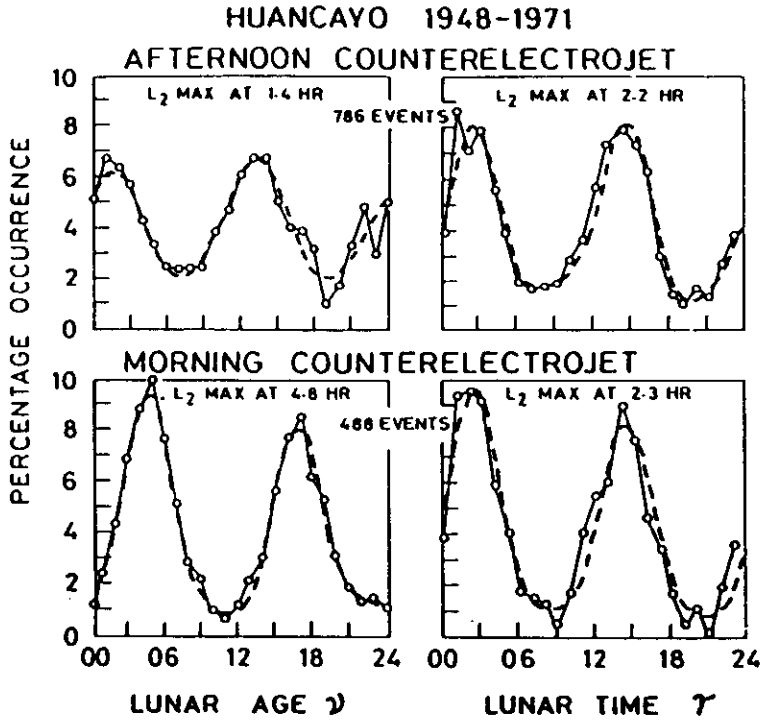

Variation of the percentage occurrence of counterelectrojet effects in the daily variation of H at Huancayo during the morning and evening hours as a function of lunar age ν and lunar time τ. (Figure is from *Rastogi* [1974b].

Fig. 38 JATP 36, 167 (1974)

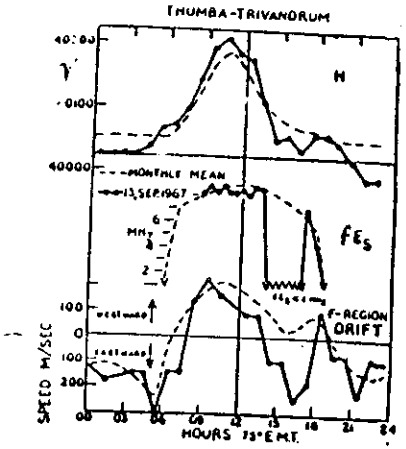

Fig. 3. Daily variations of H, fEs and East-West F-region drift at Thumba/Trivandrum on 13 September 1967 along their monthly mean variations showing the depression in H, disappearance of E_s and reversal of drift occurring simultaneously.

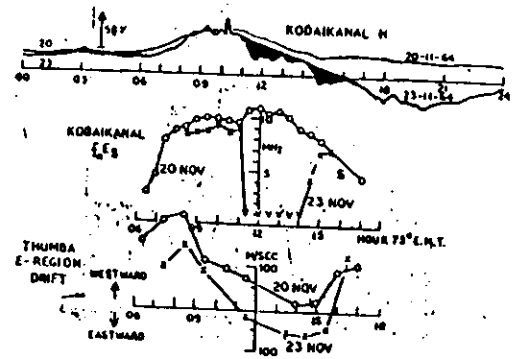

Fig. 4. Daily variations of H (Kodaikanal) f_0E_s (Kodaikanal) and E-W E-region drift (Thumba) on a quiet (20-11-1964) day and a disturbed (23-11-1964) day. Note the depressions in H disappearance of E_s and the Eastward E-region drifts occur simultaneously in time.

Fig 39

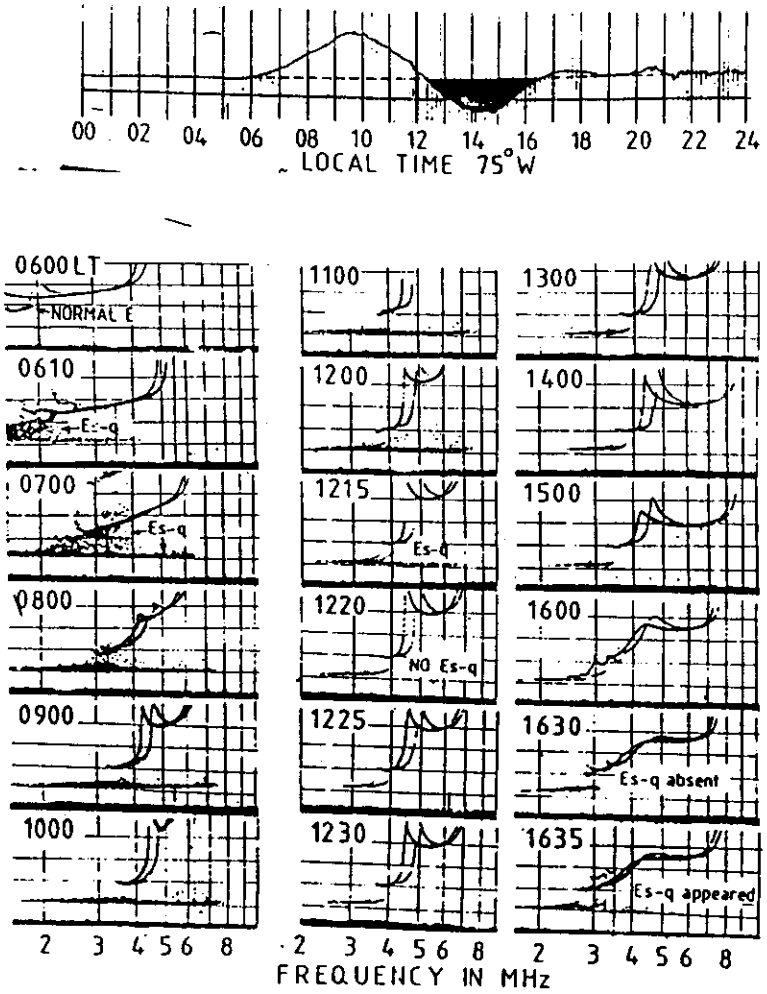

Fig. 40

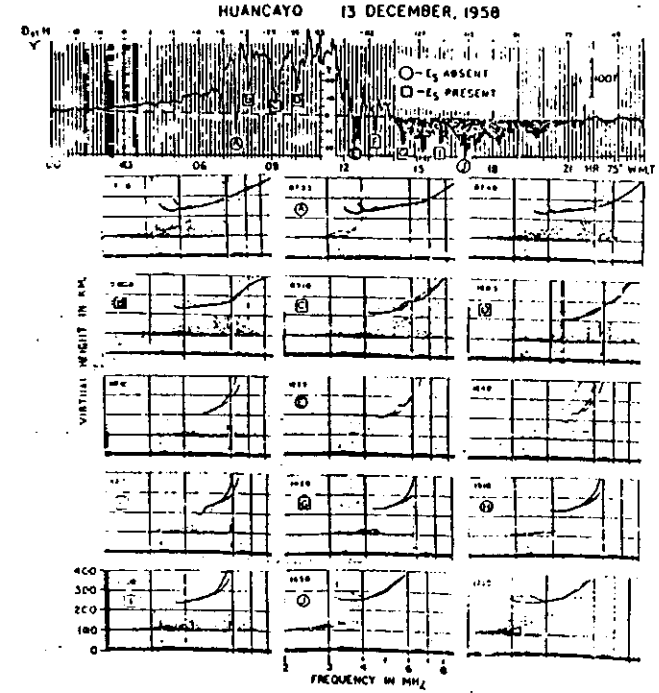

Fig. Magnetogram and ionograms at Huancayo on a magnetic disturbed day (13th December 1958 showing the disappearance of E_s at the times of sharp decreases of H.

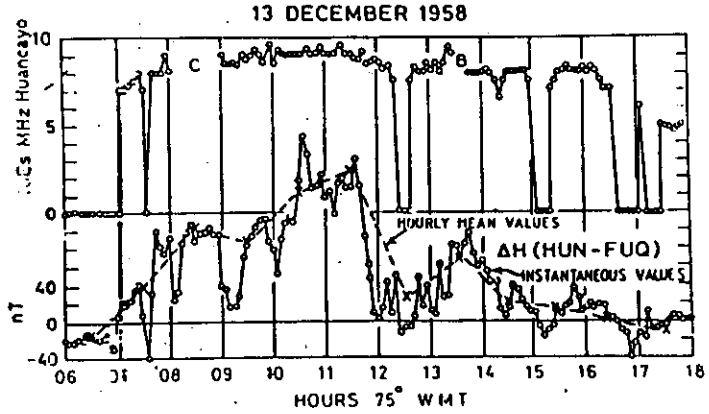

Fig. 4b

APPARENT DRIFT VECTOR IN E-REGION
THUMBA-KODAIKANAL, JUNE-JULY, 1964, 15-17 HR.

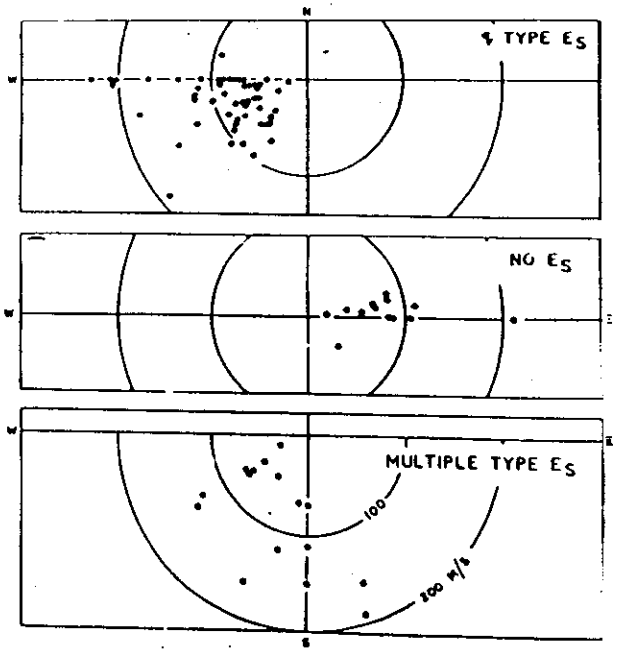

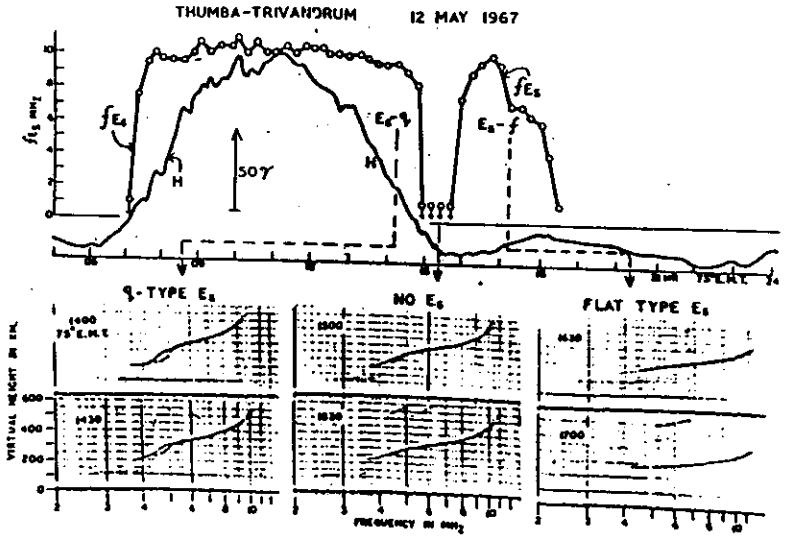

Fig 42

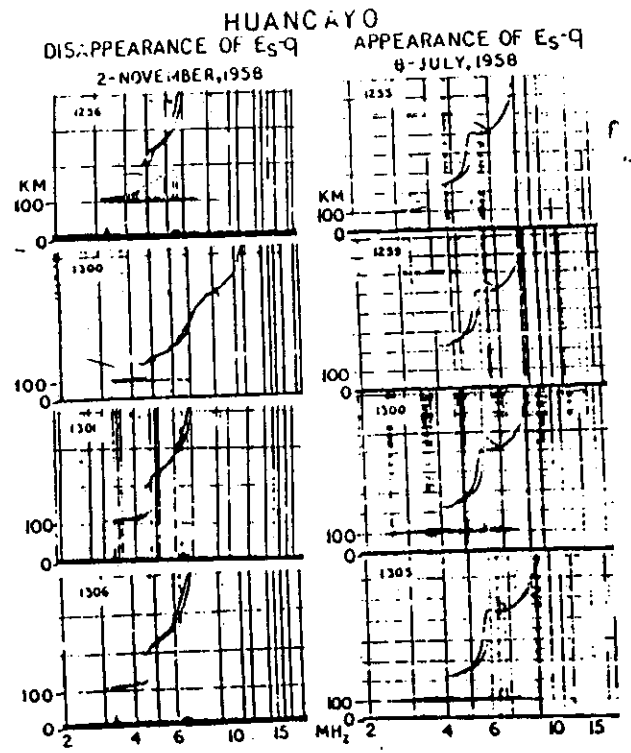

Fig.1 : The sequence of vertical sounding ionograms at Huancayo showing the sudden disappearance of Es-q between 1300 and 1301 LT on 2 November 1958 and the sudden appearance of Es-q between 1259 and 1300 LT on 8 July 1958.

Fig. 43

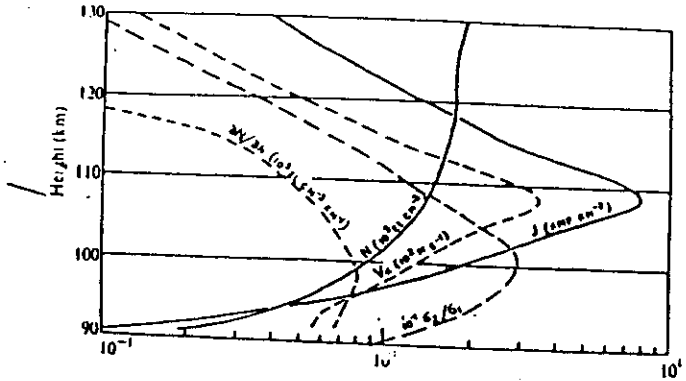

Fig. 2 Height profiles of electron density (N), electric current (J), electron drift velocity (V_d), electron density gradient ($\partial N/\partial h$) and the vertical polarization field ($E_p = \sigma_2/\sigma_1$) at the magnetic equator derived from rocket sounding data taken at 1100 h LT on March 12, 1965, off the coast of Peru (11.4° S, 81.3° W) after Maynard[7]. The electron drift is a maximum around 108 km whereas the vertical electric field is a maximum at 100 km.

3

Fig. 44

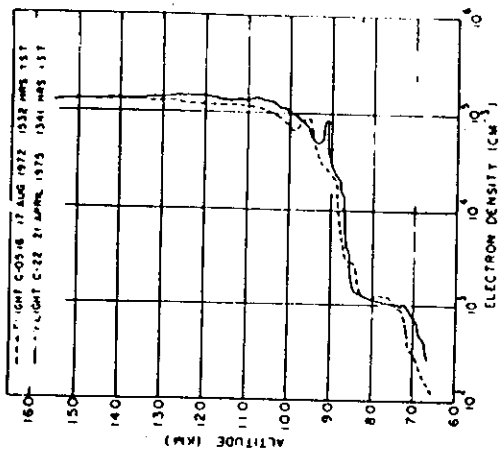

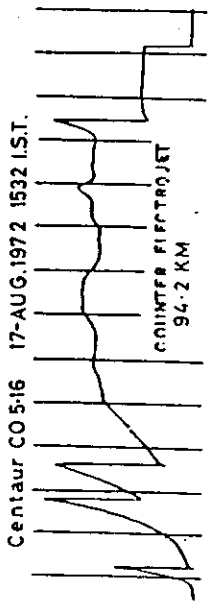

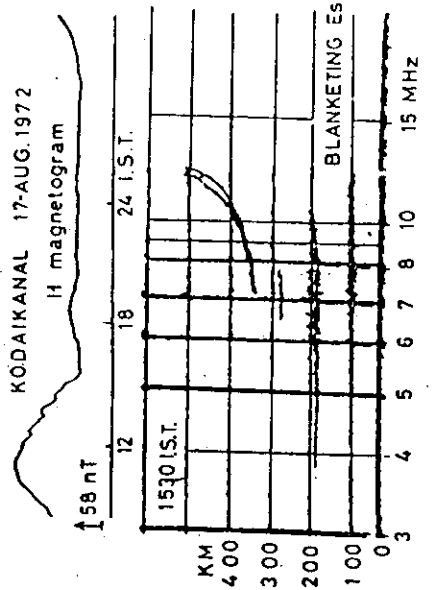

Fig. 45 After Prakash et al

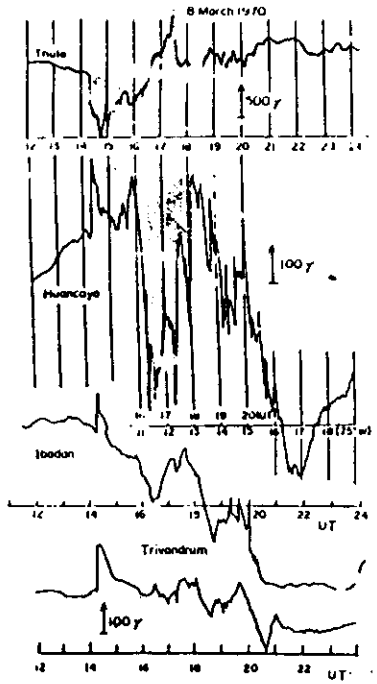

FIG. 4. THE VARIATIONS OF HORIZONTAL COMPONENT OF THE EARTH'S MAGNETIC FIELD AT EQUATORIAL STATIONS TRIVANDRUM, IBADAN AND HUANCAYO AND A STATION CLOSE TO THE NORTH POLE (THULE), DURING SC STORM STARTING AT 1417 HR UT ON 8, MARCH 1970.

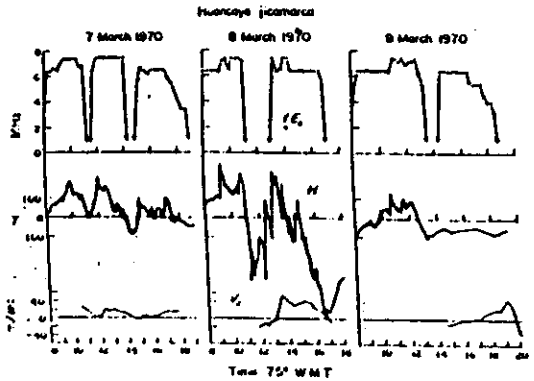

FIG. 2. VARIATIONS OF *H* FIELD AND *fE*, AT HUANCAYO COMPARED WITH THE VERTICAL *F*-REGION DRIFTS (V_z) AT JICAMARCA ON 7-9, MARCH 1970.

Fig 46

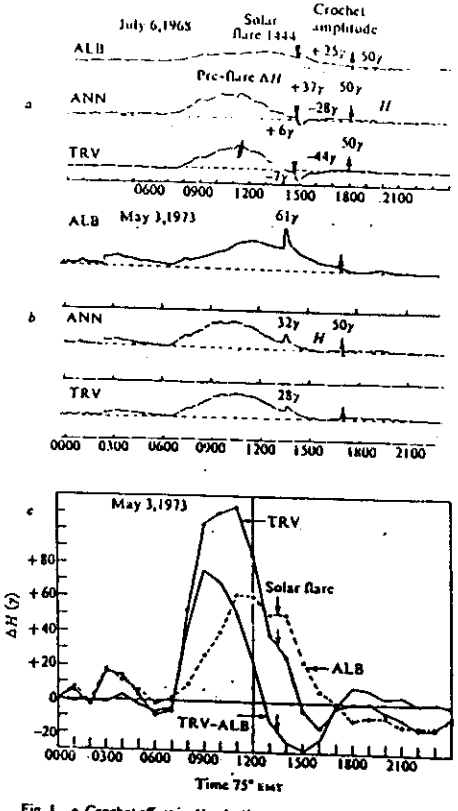

Fig. 1 *a*, Crochet effect in *H* at Indian stations during a complete counter-electrojet event on July 6, 1968 at Trivandrum (TRV), Annamalainagar (ANN), and Alibag (ALB). *b*, Crochet effect in *H* at Indian stations during a partial counter-electrojet event on May 3, 1973. *c*, Diurnal variations of the geomagnetic *H* field at TRV, ALB and TRV–ALB on May 3, 1973.

Rastogi R.G. et al. Nature, Vol 258, p 218, 1975

Fig 47

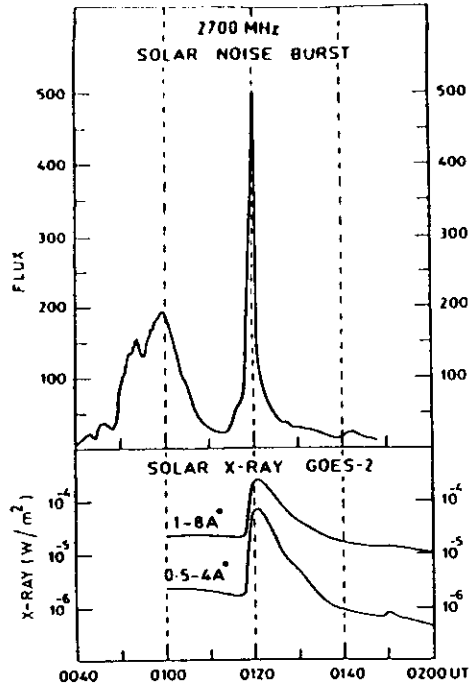

–(Top) Solar noise burst recorded at Pentincton D.C. Canada (vide *Solar Geophysical Data*) on 21 June 1980; (bottom) solar X-ray measured aboard GOES-2 satellite on 21 June 1980

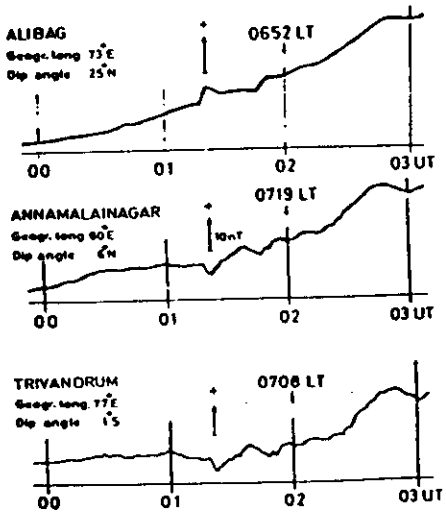

–Horizontal intensity variation recorded in the Indian zone on 21 June 1980 (Note the negative excursion at 0120 hrs UT at the electrojet stations and corresponding positive deviation at Alibag, outside and jet influence.)

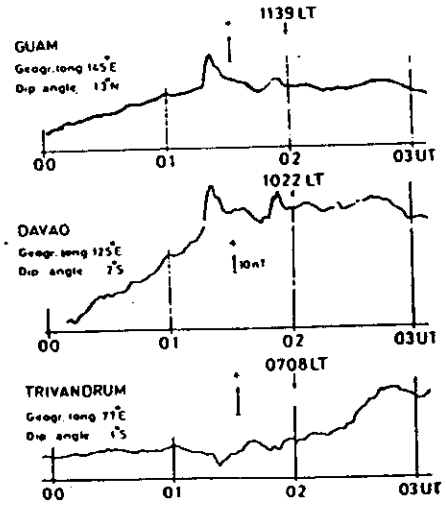

–Horizontal intensity variations recorded at equatorial latitudes in different longitude zones on 21 June 1980

Fig 48 IJRSP 10 190 (1981)

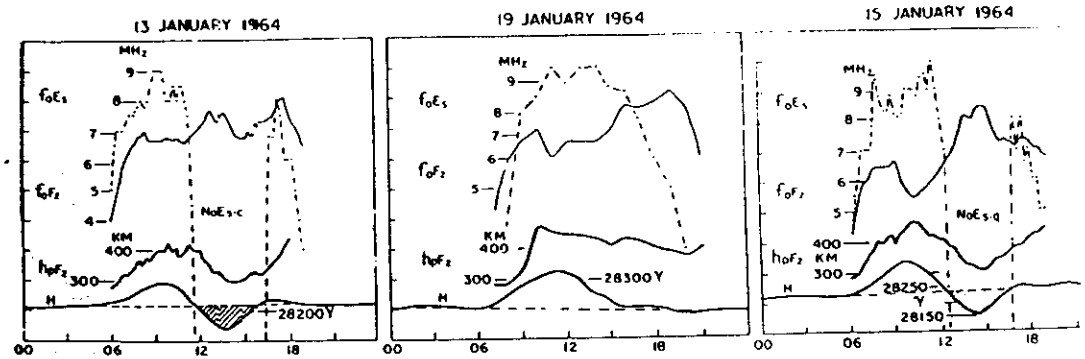

The variations of the height of peak electron density in the F region (h_pF_2), critical frequencies of the q type of E_s (f_oE_s) and of the F_2 region (f_oF_2) at Huancayo on a normal electrojet day (January 19, 1964) and on counter electrojet days (January 3 and 15, 1964).

Fig. 49 JGR 79 ₹1503 (1974)

Journal of Atmospheric and Terrestrial Physics, 1973, Vol. 35, pp. 1119–1126. Pergamon Press. Printed in Northern Ireland

Counter-electrojet and *Esq* disappearance

O. Fambitakoye
Orsay, France
R. G. Rastogi
Physical Research Laboratories, Ahmedabad-9, India
and
J. Taddagh and P. Vila
O.R.I., France

(*Received* 1 *January* 1973)

Abstract—The disappearance of *Esq* type traces from ionograms at the magnetic equator during magnetically quiet periods is related to inverted latitudinal profiles of the regular daily magnetic S_H variation (in its horizontal and vertical components). Latitude profiles obtained from a meridian chain of nine magnetometers across central Africa are compared with corresponding quarter-hourly Ionogram sequences from Fort-Archambault-Sarl. (Chad). Between 0900 and 1500 I.T, the magnetic reversal coincides exactly with the disappearance of *Esq* traces. This evidence gives additional weight to the hypothesis of a counter-electrojet current belt, located on exactly the same latitudes as the normal electrojet and probably flowing below it at the bottom of the *E*-layer. It agrees well with present theory on type II slow turbulent modes, and confirms the $V_e \wedge B$ plasma instability mechanism as the cause of *Esq* inhomogeneities at this level.

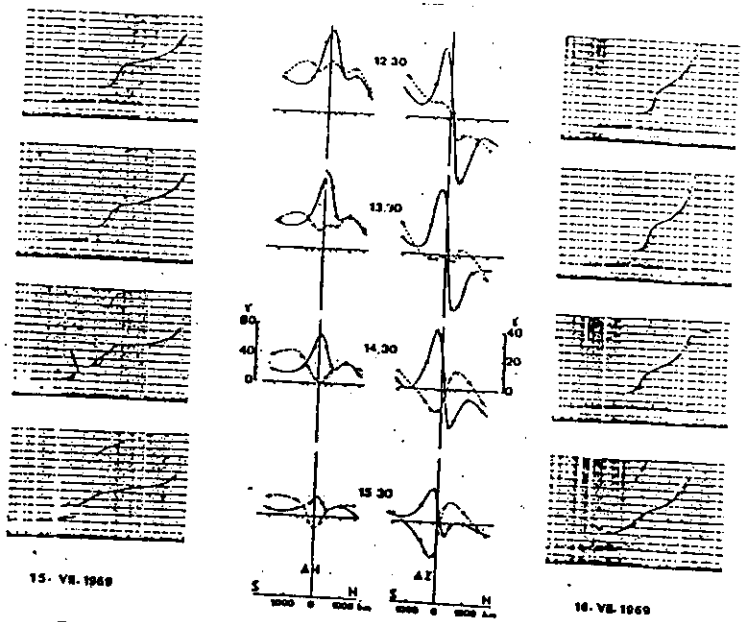

Fig. 1. Centre: latitude profiles of H and Z across the magnetic equator in central Africa. 15 July 1969, counter-electrojet day, broken line. 16 July 1969, normal day, solid line. Local time marked at the center of each horizontal row, increasing downwards. Sides: comparison with corresponding ionograms at Sarh (left) 15 July; (right) 16 July.

Fig. 50

VOL. 79, NO. 10 JOURNAL OF GEOPHYSICAL RESEARCH APRIL 1, 1974
H 1503 – 1512

Westward Equatorial Electrojet During Daytime Hours

R. G. Rastogi
Department of Physics, University of Denver, Denver, Colorado 80210

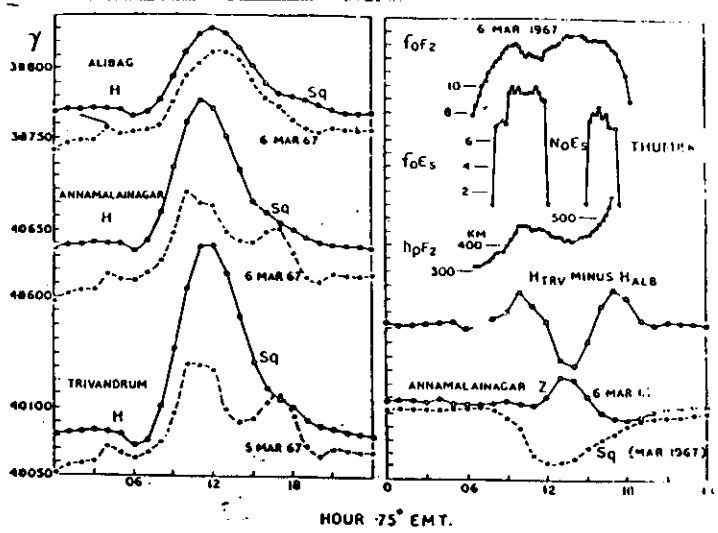

. The variations of the H field at low-latitude stations during a partial counter electrojet effect. These are compared with corresponding changes in E_s-q layer and the height of the F_2 region over the magnetic equator.

Fig. 51

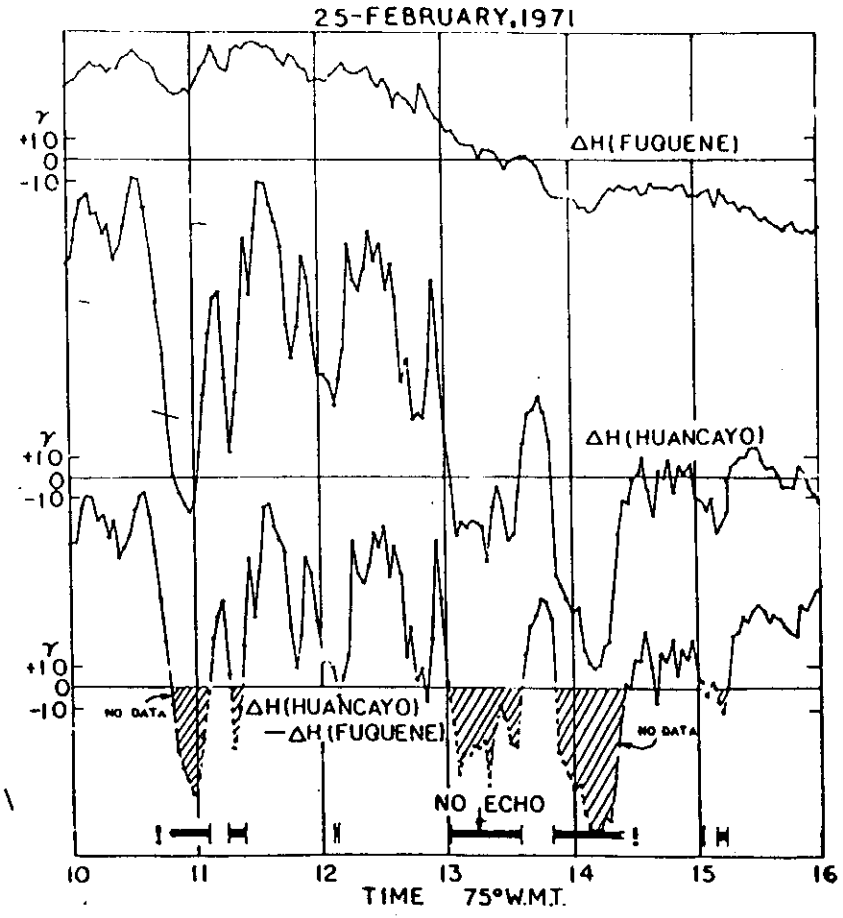
25-FEBRUARY,1971
ΔH(FUQUENE)
ΔH(HUANCAYO)
ΔH(HUANCAYO) −ΔH(FUQUENE)
NO DATA
NO ECHO
NO DATA
γ
+10
0
-10
10
11
12
13
14
15
16
TIME 75°W.M.T.

Fig 5.2

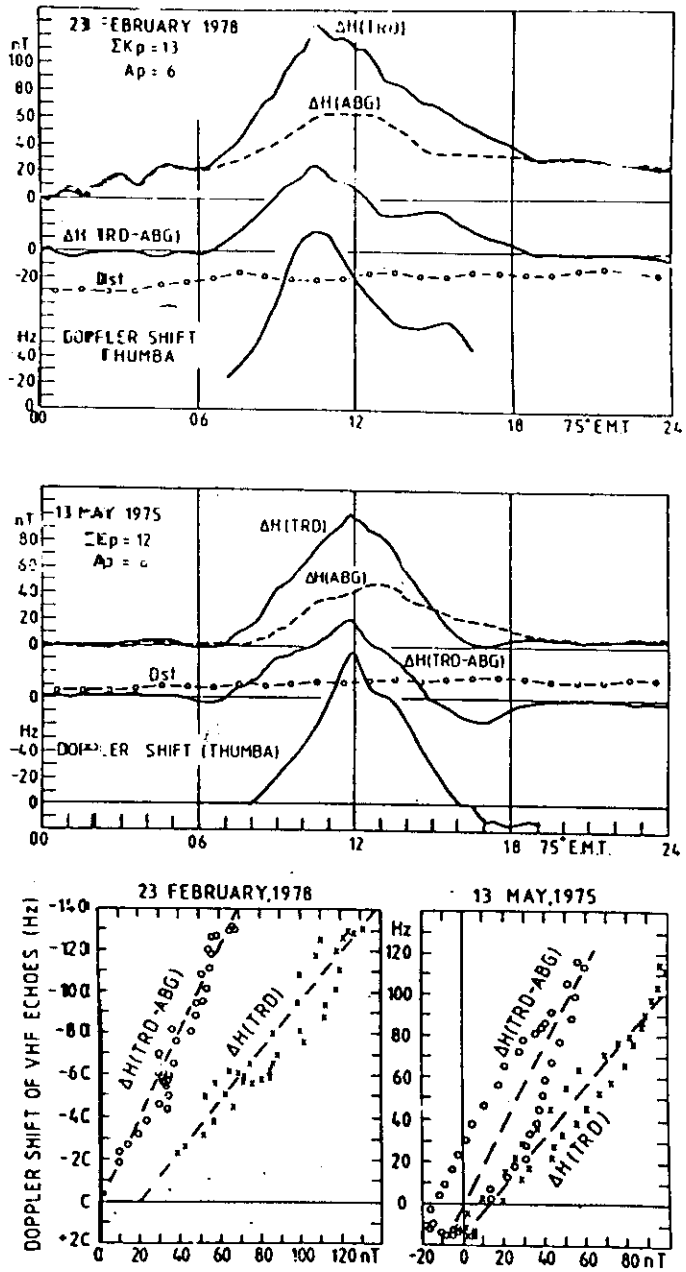
23 FEBRUARY 1978
ΣKp = 13
Ap = 6
ΔH(TRD)
ΔH(ABG)
ΔH(TRD-ABG)
Dst
DOPPLER SHIFT THUMBA
nT
Hz
00
06
12
18
75°E.M.T.
24
13 MAY 1975
ΔH(TRD-ABG)
DOPPLER SHIFT (THUMBA)
23 FEBRUARY,1978
13 MAY,1975
DOPPLER SHIFT OF VHF ECHOES (Hz)
120 nT
80 nT

Fig 5.3

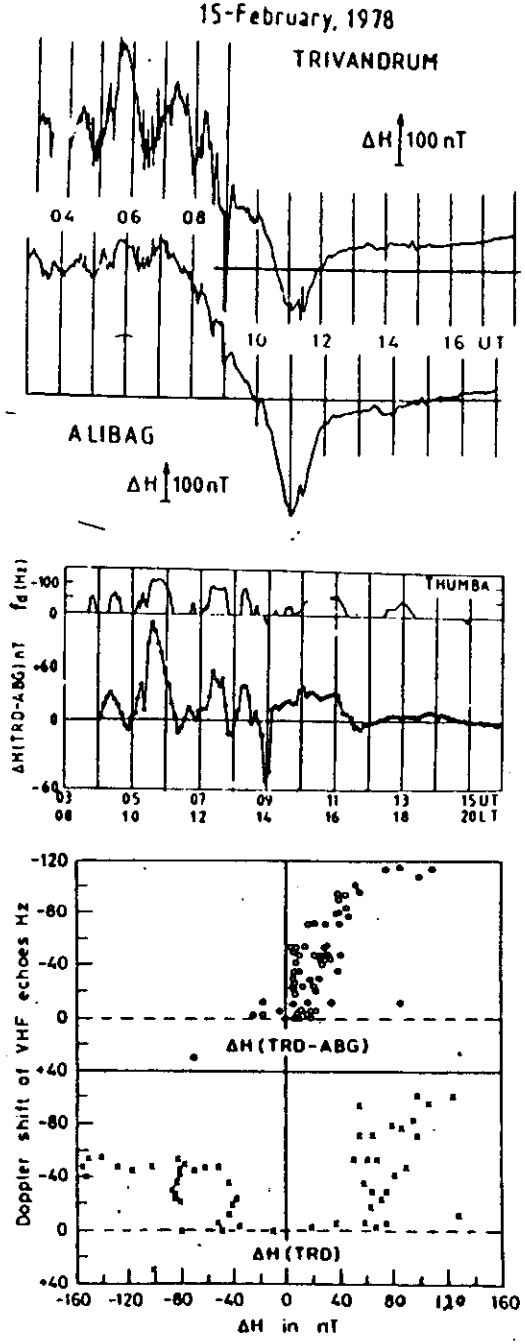

Fig 54

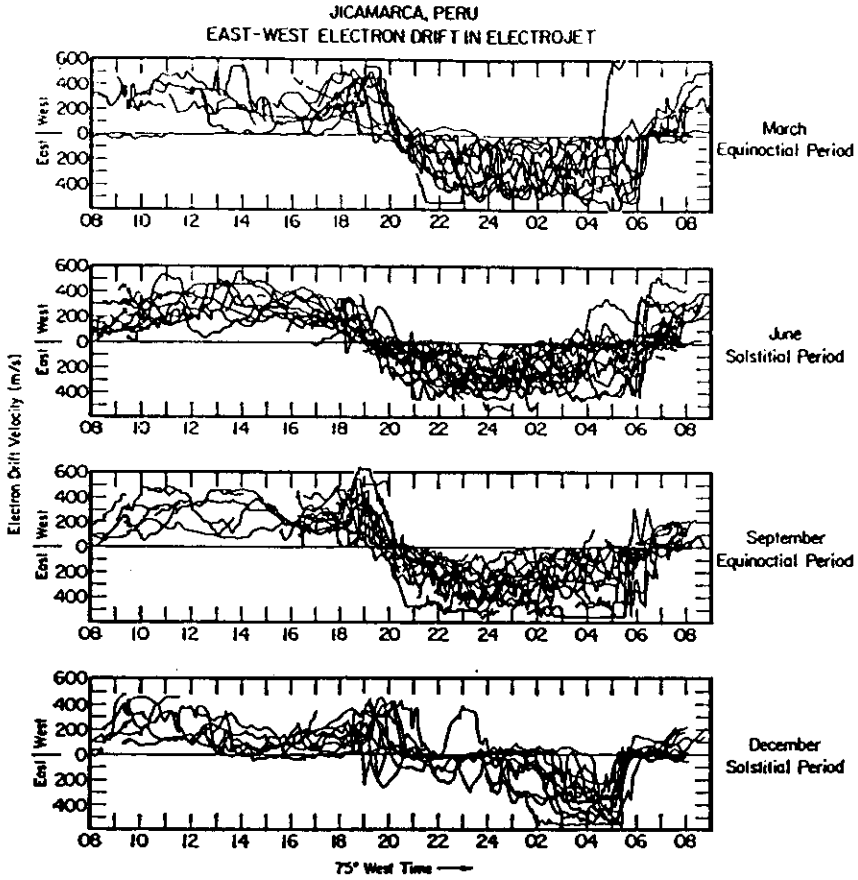

Composite of type II drift velocities obtained at Jicamarca during the period 1967–1970. (Figure is from *Balsley* [1973]. Reprinted by permission of Pergamon Press.)

Fig 55

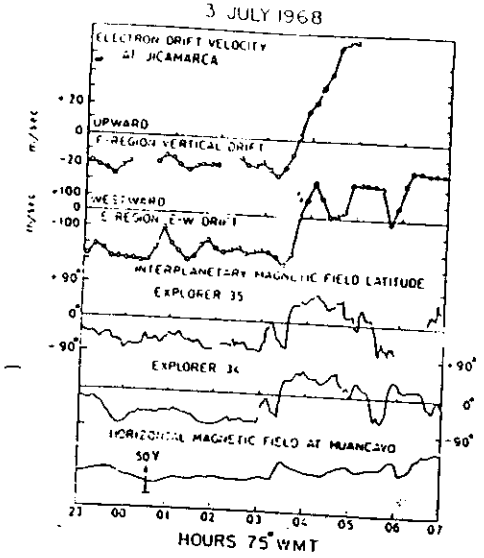

Figure 8 (*a*). The *E* region horizontal drifts and *F* region vertical drifts at Jicamarca during the nighttime on 3 July 1968 compared with the interplanetary magnetic field latitude at Explorer 34 and 35 satellites as well as the geomagnetic *H* field at ground observatory, Huancayo.

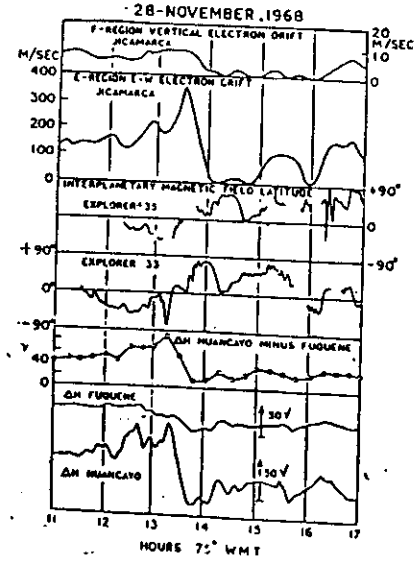

Figure 6 (*a*). The horizontal *E* region electron drifts and vertical *F* region plasma drifts at Jicamarca on 28 November 1968 compared with the changes in the latitude of interplanetary magnetic field at satellites Explorer 33 and 35. The geomagnetic fields at ground observatories Huancayo and Fuquene are also shown for comparison.

Fig 6

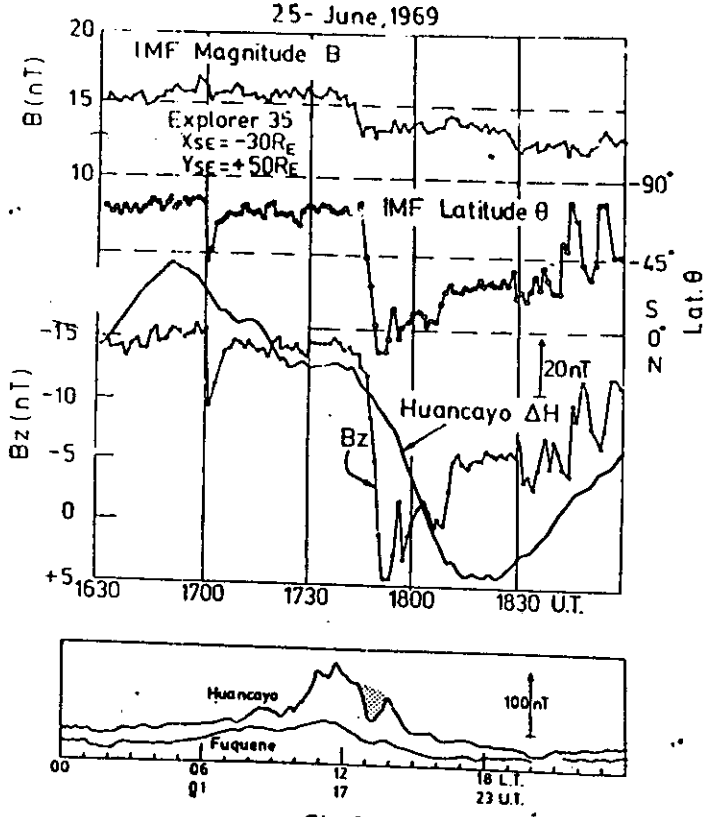

Fig 8

Fig 7

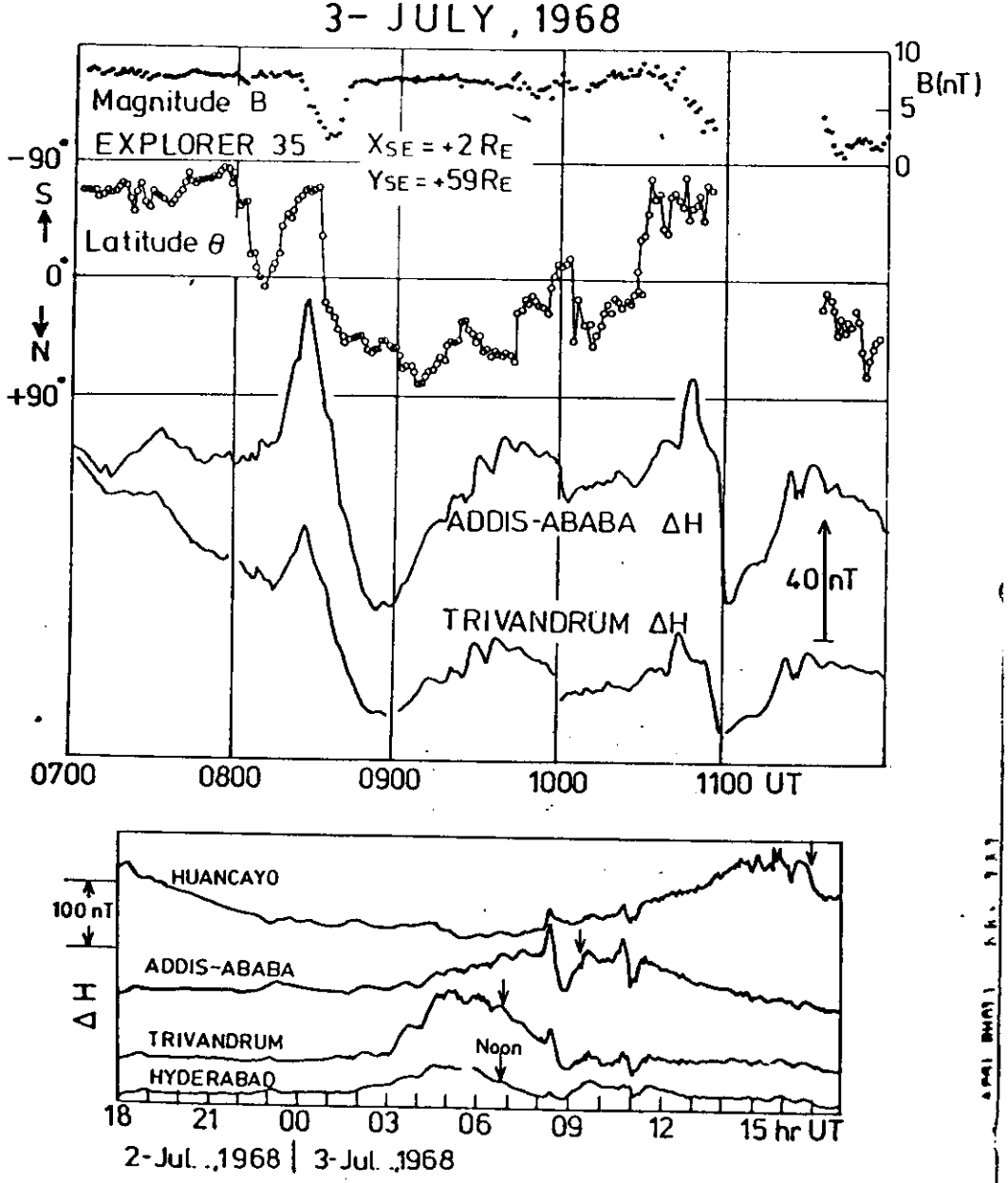
3- JULY , 1968
Magnitude B
EXPLORER 35
XSE = +2 RE
YSE = +59RE
Latitude θ
-90° S
0°
N +90°
10
5
0
B(nT)
ADDIS-ABABA ΔH
TRIVANDRUM ΔH
40 nT
0700
0800
0900
1000
1100 UT
HUANCAYO
100 nT
ADDIS-ABABA
TRIVANDRUM
HYDERABAD
Noon
ΔH
18
21
00
03
06
09
12
15 hr UT
2-Jul. .,1968 | 3-Jul. .,1968

Fig 6 B

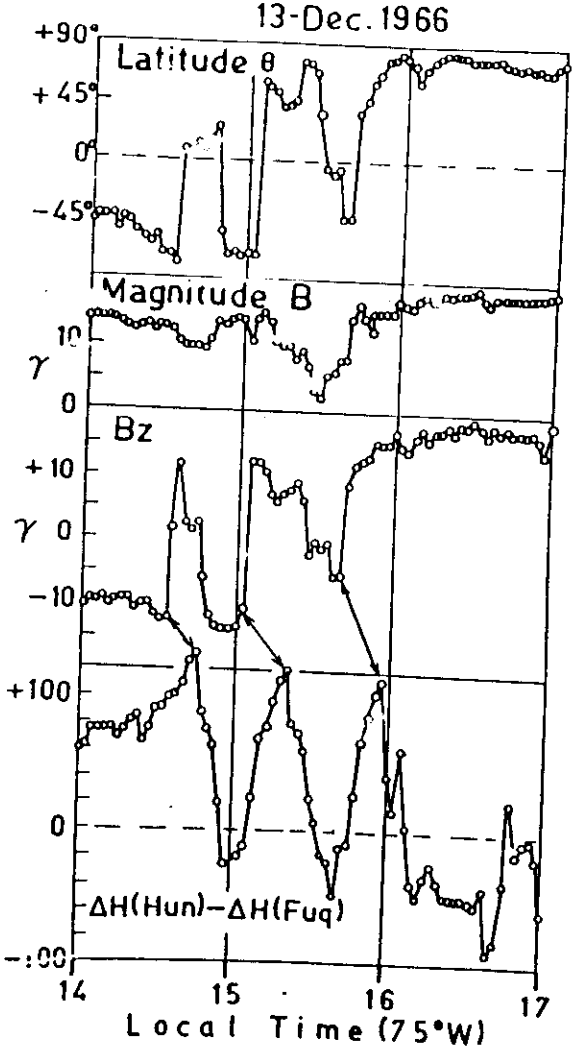
13-Dec. 1966
+90°
Latitude θ
+45°
0°
-45°
Magnitude B
γ
10
0
Bz
+10
γ 0
-10
+100
0
ΔH(Hun)-ΔH(Fuq)
-100
14
15
16
17
Local Time (75°W)

Fig 5 9

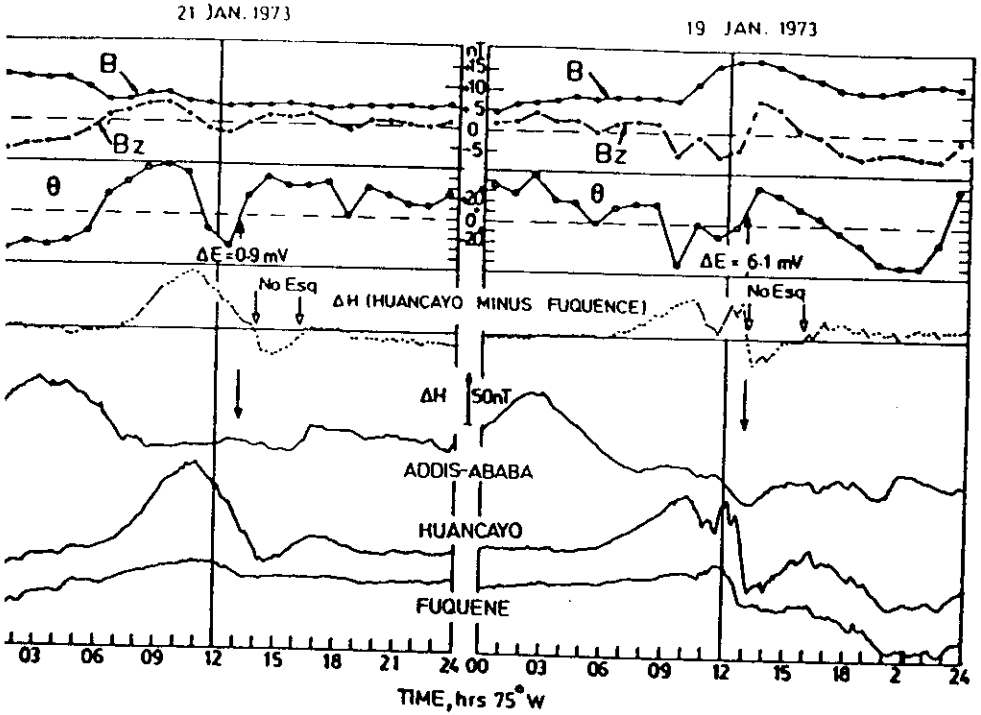

–Tracings of the magnetograms at Huancayo, Fuquene, Addis Ababa, Huancayo minus Fuquene and the hourly means of IMF components B, θ and Bz on 21 and 19 January 1973 [The counter electrojet at Huancayo on 21 January 197[illegible] was of tidal origin while sudden decrease of H at Huancayo, Fuquene and Addis Ababa at 1300 hrs (75°WMT) on 19 Jan. 1973 was due to northward turning of Bz in the presence of a large value of B.]

Fig. 6a

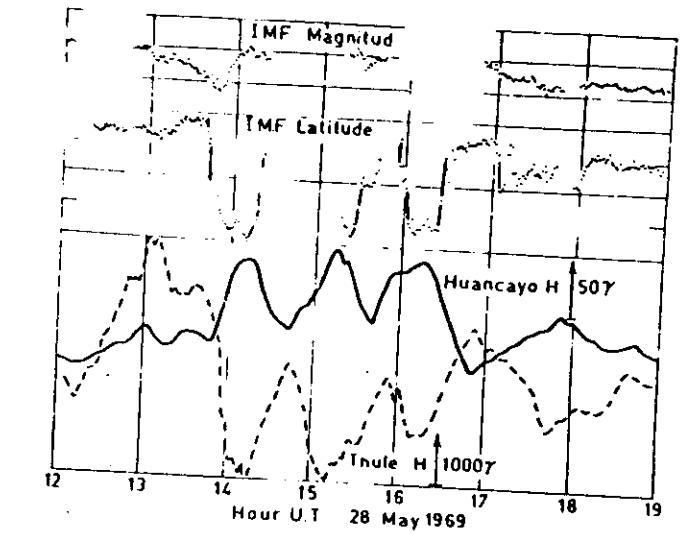

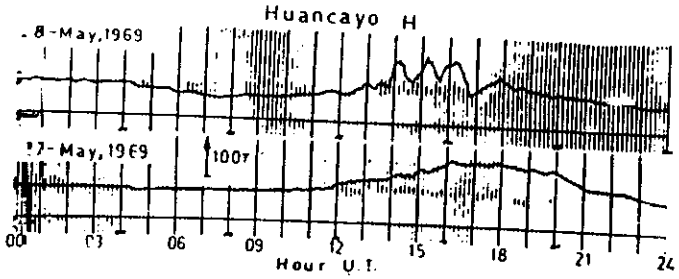

Fig 6 1

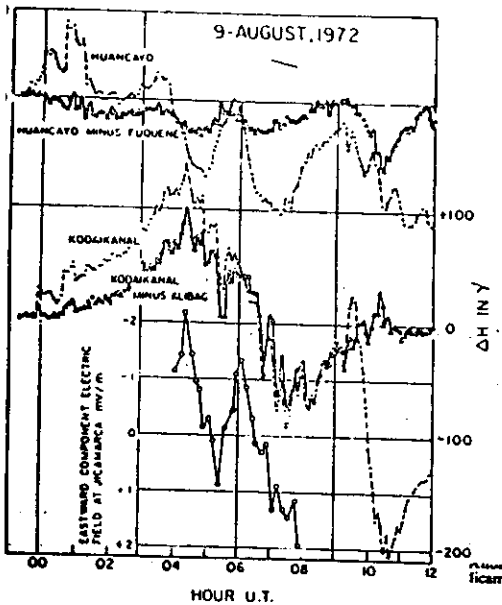

Variations of the geomagnetic H field at Huancayo, Huancayo minus Fuquene, Kodaikanal, Kodaikanal minus Alibag compared with the corresponding values of the eastward electric field at Jicamarca on 9 August 1972.

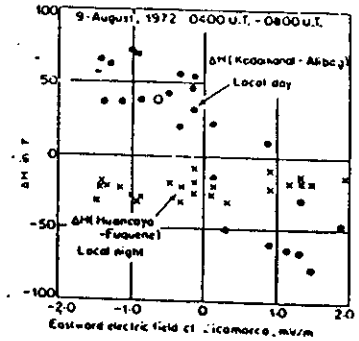

Plots of ΔH (Huancayo minus Fuquene) and ΔN (Kodaikanal minus Alibag) compared with the corresponding values of the eastward electric field at Jicamarca.

Ref. R.G. Rastogi, Proc. Ind. Acad. Sci. 86 A 409, (1977)

Fig 62

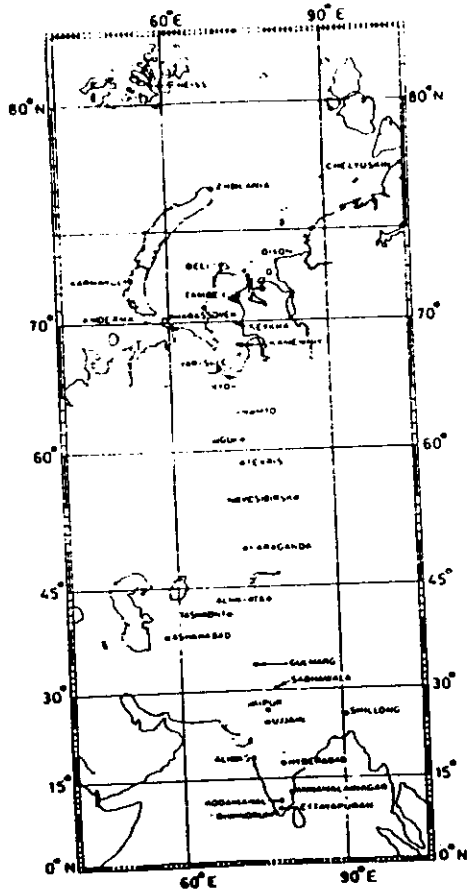

Map showing the locations of Indian and Soviet magnetometer stations in the 145° geomagnetic meridian zone.

Fig 63

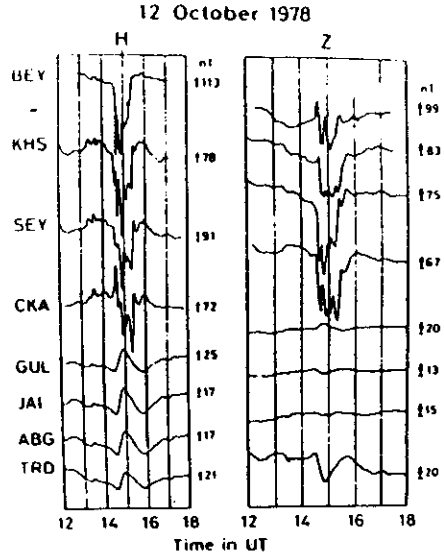

Magnetospheric substorm event of 12 October 1978. The length of the arrow for each station gives the scale factor.

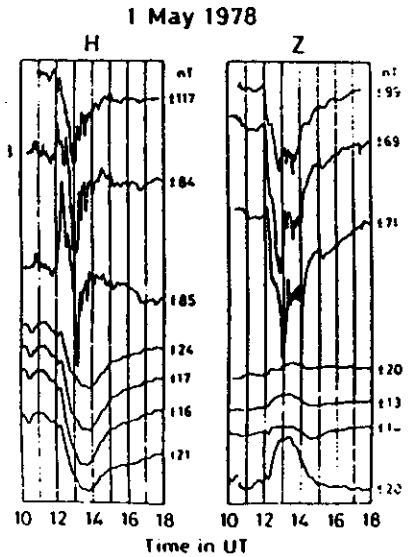

Magnetospheric substorm event of 1 May developing during local evening hours. Format as for figure 2.

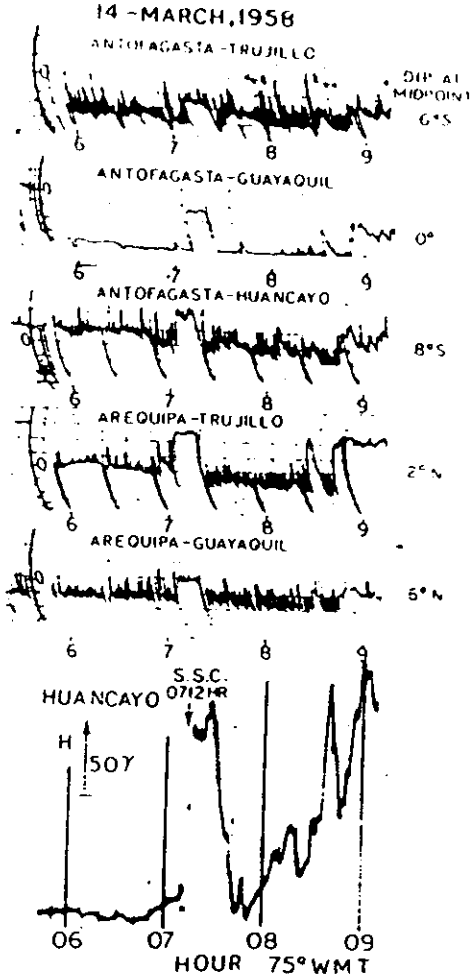

Changes in H at Huancayo associated with the ssc at 0712 a 75° WMT on March 14, 1958, and its effect on VHF scatter ›pagation paths in Peru.

Fig 64

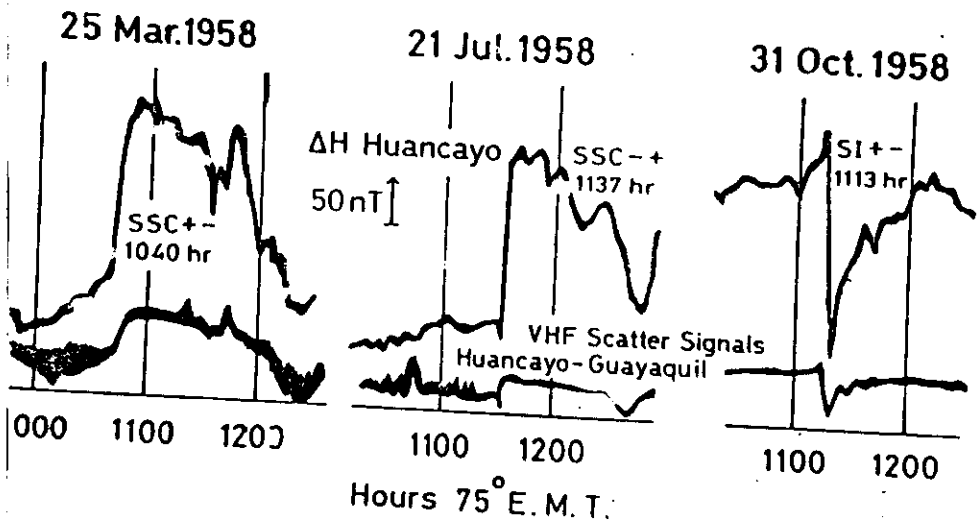

Fig 65

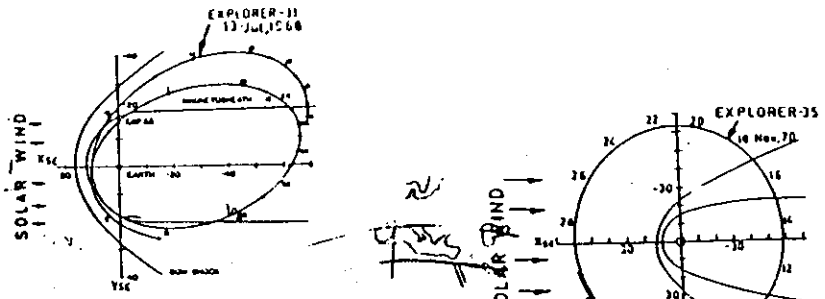

13-Jul,1968

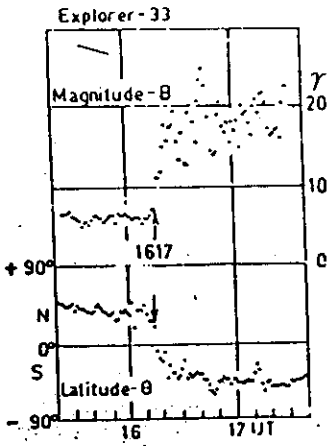

18-Nov,1970

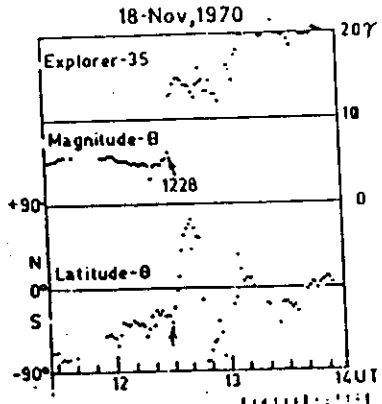

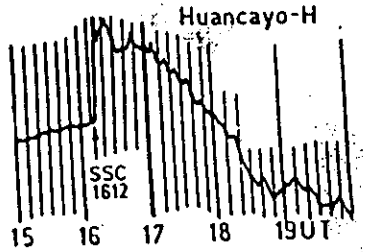

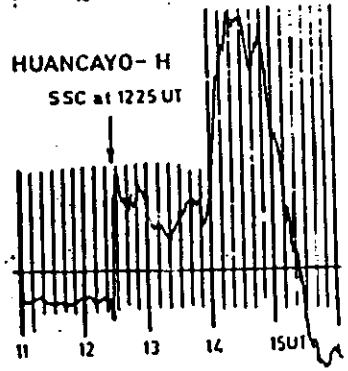

Fig 66